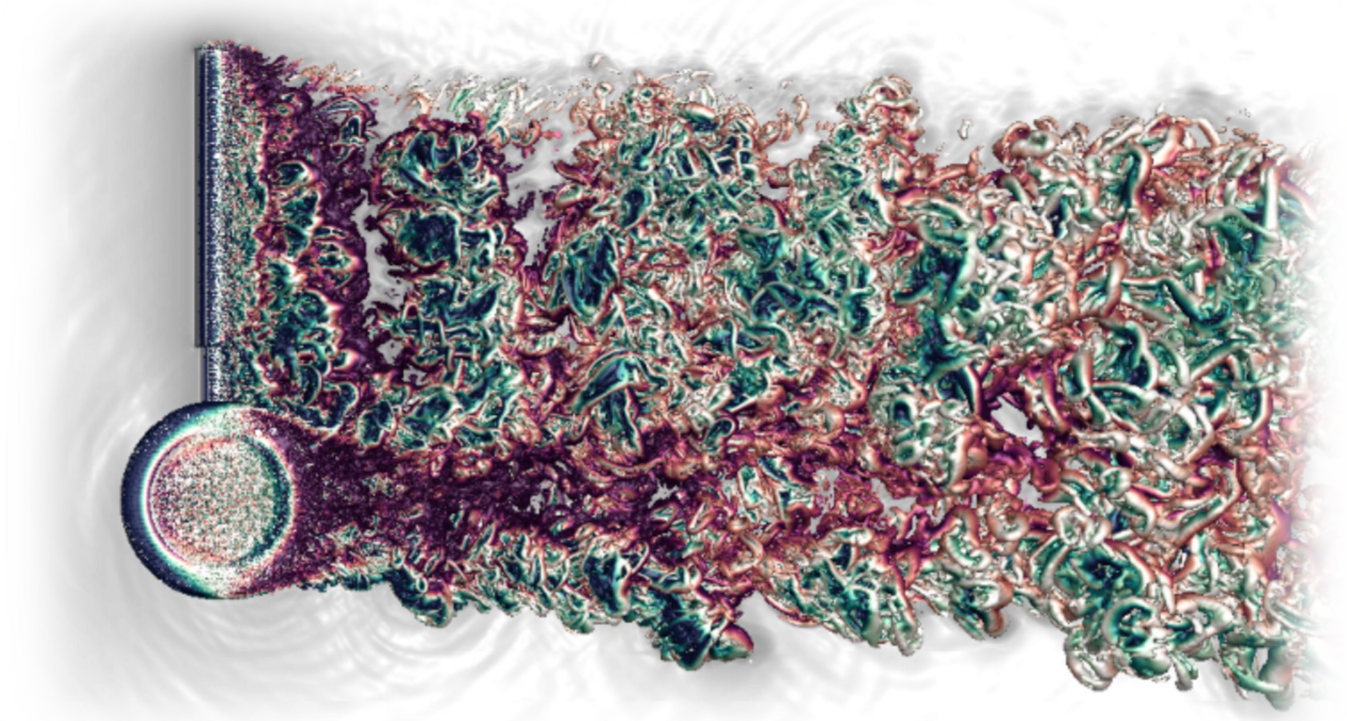
Predictions of LAGOON Nose Landing Gear Aeroacoustics using Wall-Modeled Large-Eddy Simulations

Man-Long Wong, Gaetan Kenway, Aditya Ghate, Gerrit-Daniel Stich, and Cetin Kiris

Computational Aerosciences Branch
NASA Ames Research Center



Advanced Modeling and Simulation (AMS) Seminars
NASA Ames Research Center, Aug 30th 2022

* Wong, Man Long, et al. "Predictions of LAGOON Nose Landing Gear Flow and Noise using Wall-Modeled Large Eddy Simulations." *28th AIAA/CEAS Aeroacoustics 2022 Conference*. 2022.

Outline

- Scope of this work
- Description of a benchmark landing gear problem - LAGOON
- Numerical and meshing approaches for wall modeled large-eddy simulation (WMLES)
- WMLES results
  - Near-field results without explicit numerical tripping
  - Near-field results with explicit numerical tripping
  - Far-field acoustic results
- Summary

Scope of this work

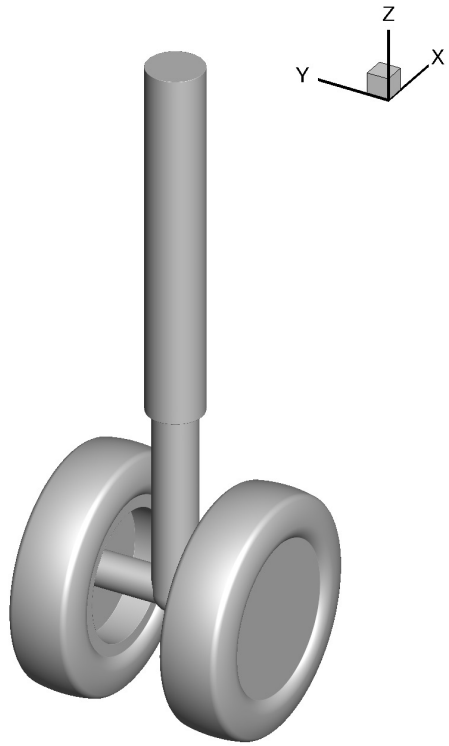
- Commercial aircraft noise has adverse effects on the quality of life and health of residents near major airports
- As noise regulations are more stringent, design of more quiet aircrafts is critical
- With the development of more quiet aircraft engines (e.g. with large bypass ratios), airframe noise is becoming a more dominant noise source during approach or landing of commercial aircrafts
- The landing gear noise is one of the most prominent sources of airframe noise
- The landing gear noise has both the tonal and broadband characteristics which pose challenges on the accurate numerical predictions of noise levels during the design of low noise components using computational fluid dynamics (CFD) and computational aeroacoustics (CAA) tools
- In this work, the capability of the wall-modeled large-eddy simulation (WMLES) approach on predicting landing gear noise is investigated
  - Near-field noise and flow obtained directly with CFD simulation
  - Far-field noise approximated with the impermeable Ffowcs Williams-Hawkings (FWH) acoustic analogy approach

LAGOON landing gear problem description

- **LA**nding-**G**ear n**O**ise database for CAA validati**ON** (LAGOON) [1]
  - A popular landing gear benchmark problem for validation and verification of different CFD and CAA methodologies
  - Flow past a 1:2.5 scaled model of Airbus A320 aircraft nose landing gear
  - Freestream wheel Reynolds number $\boldsymbol{Re_D = 1.55\times10^6}$
  - Freestream Mach number $\boldsymbol{Ma_\infty = 0.23}$

- The nose landing gear has a simplified shape which consists of:
  - 2 wheels with diameter $\boldsymbol{D = 0.3\ \mathrm{m}}$
  - Lower and upper struts (with diameters of 55 mm and 71 mm)
  - Axle (with diameter of 46 mm)

- Mean and unsteady aerodynamic measurements in ONERA's F2 closed-loop wind tunnel
- Far-field acoustic data measured in ONERA's CEPRA 19 (C19) open-jet wind tunnel (mean and unsteady wall pressure data also collected)



1. Manoha, E., and Caruelle, B., "LAGOON Simplified (2-Wheel) Nose Landing Gear Configuration# 1 Experimental Database," Tech. rep., Technical Report, 2011.

Overview

- In the BANC-III workshop[1], near-field and far-field results from various groups with different CFD methodologies were compared:
  1. Meshing strategies:
     - Multi-block structured mesh
     - Unstructured mesh
     - Cartesian octree mesh [only used with lattice-Boltzmann method (LBM)]
  2. Turbulence modeling:
     - Hybrid Reynolds Averaged Navier-Stokes (RANS)/large-eddy simulation (LES) [Majority]
     - Wall-modeled LES (WMLES) with wall-stress models [Minority]

- Among three meshing methodologies, the use of Cartesian octree meshing with the immersed boundary method is the most attractive approach since it can save a large amount of labor cost in the preparation of the mesh for a realistic landing gear with hydraulic lines, fasteners, hinges, etc., which is challenging for body-fitted meshing

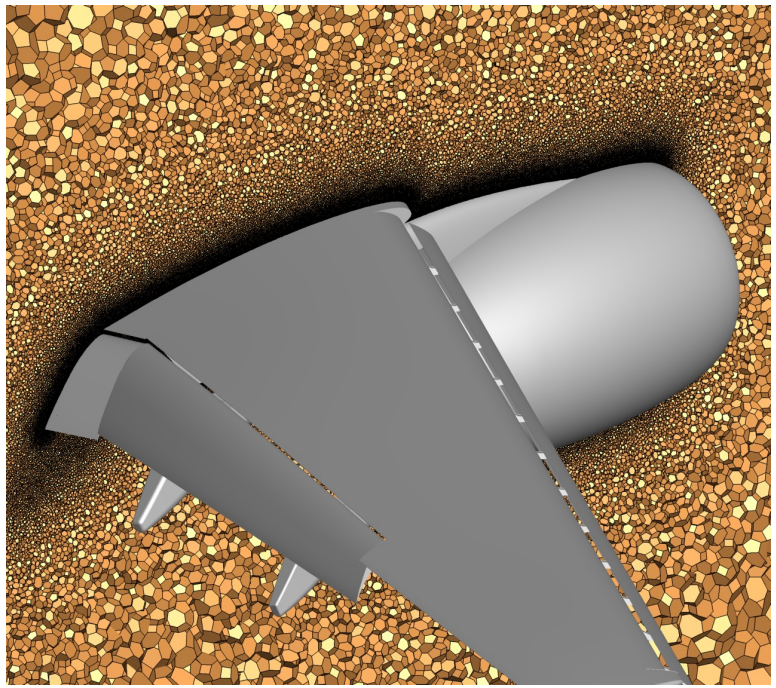
- In this presentation, predictions of both near-field and far-field aeroacoustics with Navier-Stokes Cartesian simulations using the WMLES and immersed boundary capabilities in the Launch, Ascent, and Vehicle Aerodynamics (**LAVA**) framework are presented

- The results can be used to inform the airframe noise community on the use of the WMLES with immersed boundary octree meshes for the design of low noise components

1. Manoha, E., and Caruelle, B., "Summary of the LAGOON solutions from the Benchmark problems for Airframe Noise Computations-III Workshop," 21st AIAA/CEAS aeroacoustics conference, 2015, p. 2846

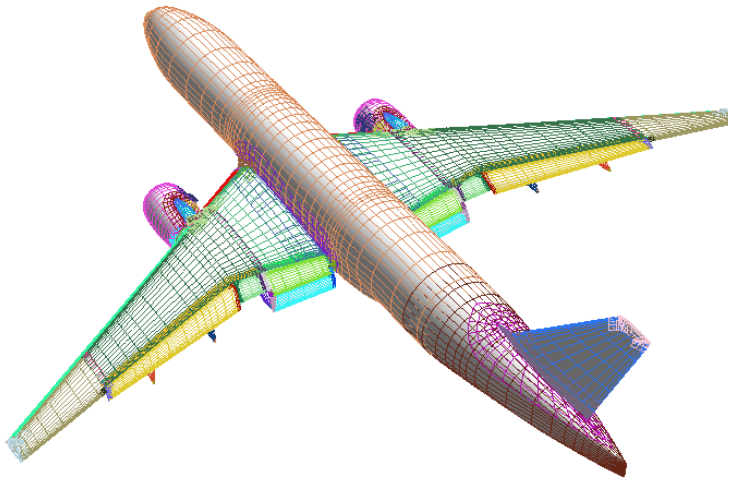
LAVA CFD Grid Paradigms[1]

Unstructured



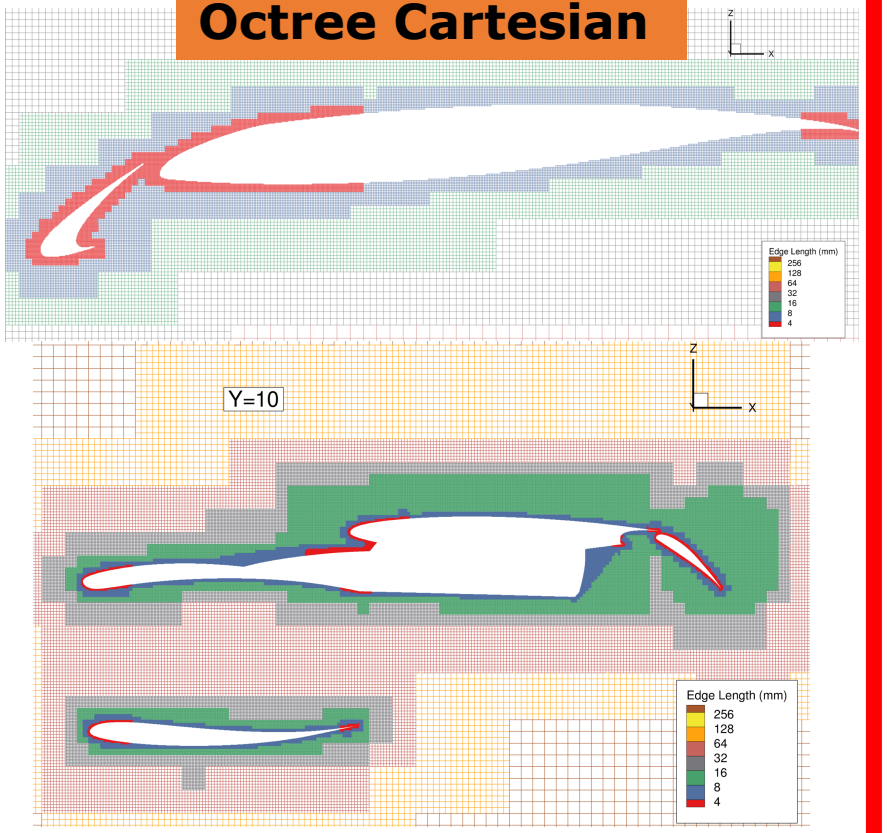
- Partially automated grid generation
- Body fitted grids
- High grid quality can be challenging
- High computational cost
- Higher order methods yet to fully mature

Structured Curvilinear



- High quality body fitted grids
- Low computational cost
- Reliable higher order methods
- Grid generation largely manual and time consuming

Octree Cartesian



- Automatic volume grid generation
- High-order methods are efficient and mature
- Isotropic grid cells non-ideal for resolving boundary layer
- Wall modeling is the key

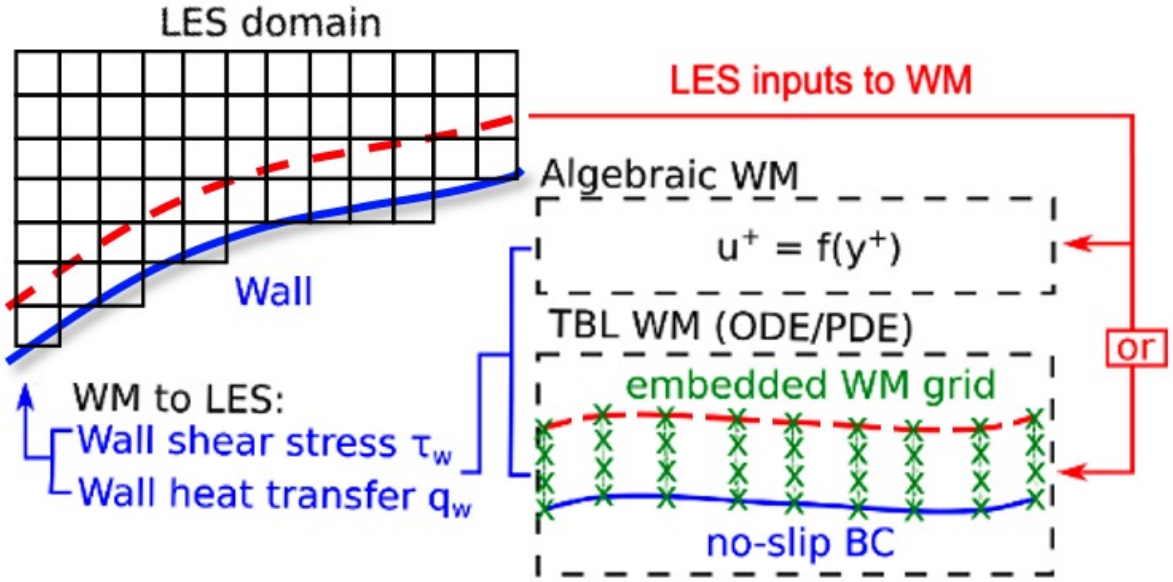
1. Kiris et.al. “Computational Framework for Launch, Ascent, and Vehicle Aerodynamics (LAVA)”, 2016

Numerical Setup in Cartesian LAVA

- Simulations using the compressible Navier-Stokes equations with the Vreman subgrid-scale (SGS) model are conducted
- The convective flux vectors are discretized with a 4^{th} order midpoint-and-node central finite difference scheme for lower aliasing errors
- The midpoint flux vectors are computed with the HLLC Riemann solver using left- and right-biased interpolated primitive variables
- 4^{th} order central interpolation blended with 3^{rd} order upwind-biased interpolation
- Overall convective flux discretization is essentially central and has low dissipation in turbulent regions
- Viscous and diffusive flux vectors are evaluated at the midpoints using 2^{nd} order accurate staggered finite differencing, followed by 2^{nd} order divergence
- 3^{rd} order TVD Runge-Kutta scheme used for time stepping
- CFL number ≈ 1.5 used for all simulations

Wall Modeled Immersed Boundary Method

- Ghost cell immersed boundary method (IBM) used with surface triangulations which define the location of solid body
- Grid cells inside the body are filled with appropriate flow data for imposing no-penetration boundary conditions for convective fluxes
- LES solutions are computed all the way to the walls with wall modeled stress and heat flux boundary conditions
- Wall model uses LES solutions close to the wall as outer boundary conditions
- Algebraic equilibrium wall model used to obtain approximate solutions to the ODE-based equilibrium WM



1. Stich, G.-D., Ghate, A. S., Housman, J. A., and Kiris, C. C., “Wall Modeled Large Eddy Simulations for NASA’s jet noise consensus database of single-stream, round, convergent jets.” AIAA SCITECH 2022 Forum, 2022, p. 0684.
2. Ghate, Aditya S., et al. "A Wall-Modeled LES Perspective for the High Lift Common Research Model Using LAVA." *AIAA AVIATION 2022 Forum*. 2022.

Gridding and Simulation Strategies

- Six different Cartesian octree grids employed for grid sensitivity study
- Finest grid deployed around all geometry components where the number of cells for the 3 finest grids, grids D, E, and F, per wheel diameter are 500, 1000, and 1500 respectively [230 cells per axle diameter for grid F]
- Simulations in an open domain are run for 100 convective time units (CTUs) to flush out initial transients; data collected for the next 200 CTUs

Higher resolution

Grid	Number of mesh levels	Min grid spacing (mm)	Number of grid cells (M)	Number of surface elements (M)	Time step size (μs)	CPU hours per 1 ms of physical time*
A	11	4.8	2.197	5.763	~ 5.79	1.322
B	12	2.4	6.130	5.763	~ 2.82	2.385
C	13	1.2	22.16	5.763	~ 1.37	9.152
D	14	0.6	100.5	5.763	~ 0.70	55.32
E	15	0.3	309.0	15.94	~ 0.35	303.0
F	16	0.2	737.9	63.76	~ 0.23	920.5

*simulations were conducted with the Intel Skylake processors (20-core Xeon Gold 6148 model)

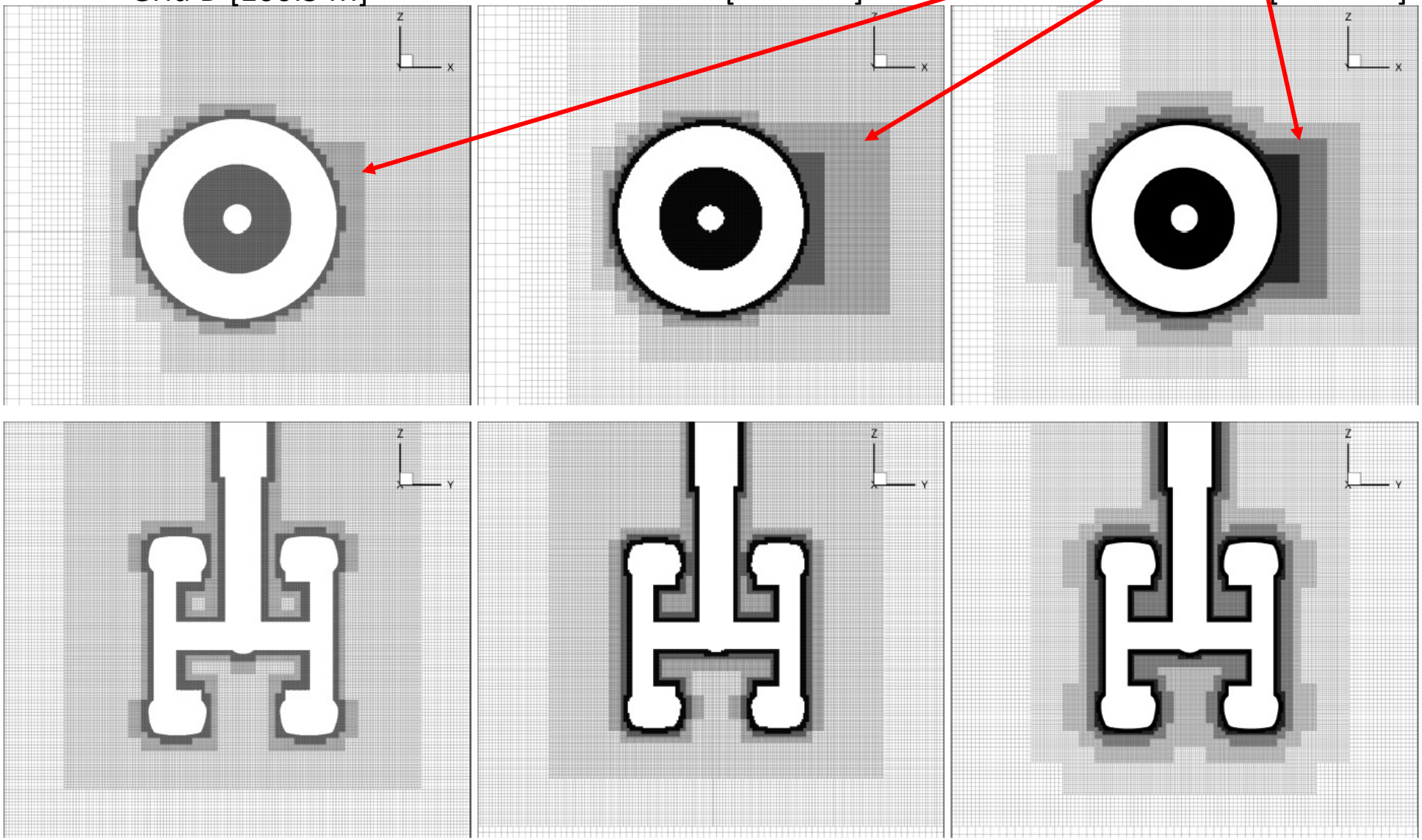
Cartesian Octree Grids

Gradual coarsening of the wake grid

Grid D [100.5 M]

Grid E [309.0 M]

Grid F [737.9 M]

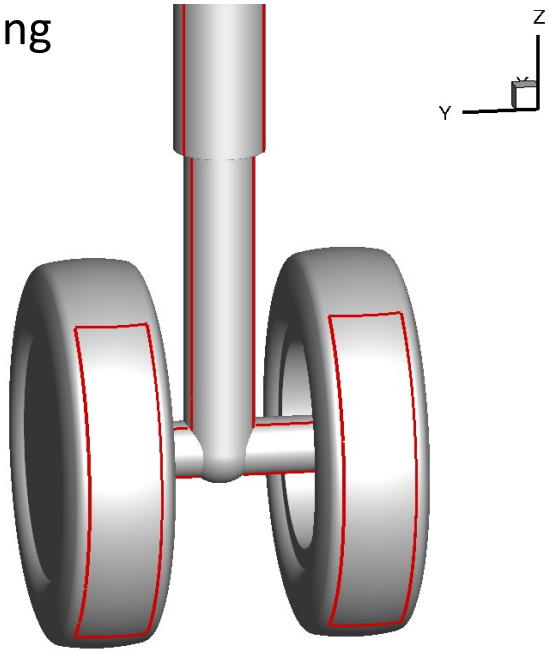


- Finest grid deployed around all geometry components with constant physical thickness

Simulation Cases: without/with Tripping for Transition

- During the experiments, laminar to turbulent transition physical tripping strips imposed on wheels, axle and struts
- Some groups in the BANC-III workshop also explicitly tripped the flow to mimic the effects of strips in the experiments
- Explicit numerical tripping also attempted in this work to reproduce the tripping effects in the experiments
- Two simulation cases with tripping:
    1. Only tripping on axle and main strut imposed
    2. Tripping imposed at all tripping locations in experiments

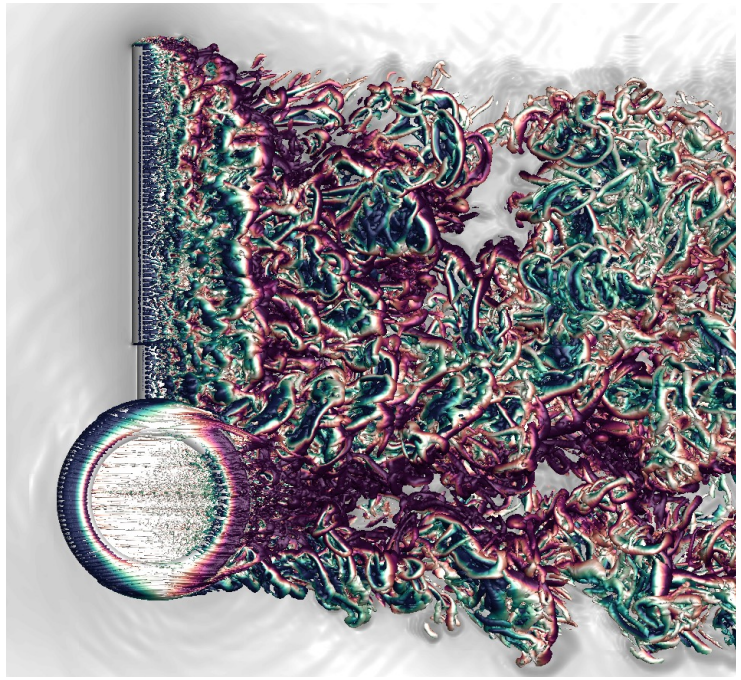
- **Part I:** analysis of near-field simulation results without tripping (grids A – F)
- **Part II:** analysis of near-field simulation results with tripping (grids D – F)
- **Part III:** analysis of far-field results using an acoustic analogy (all cases)



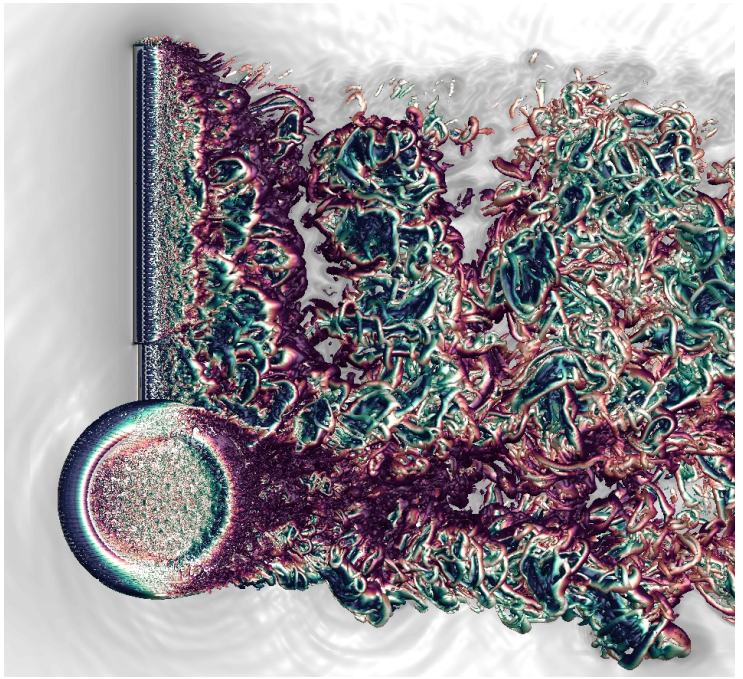
Locations of tripping lines in experiments colored in red

Visualizations

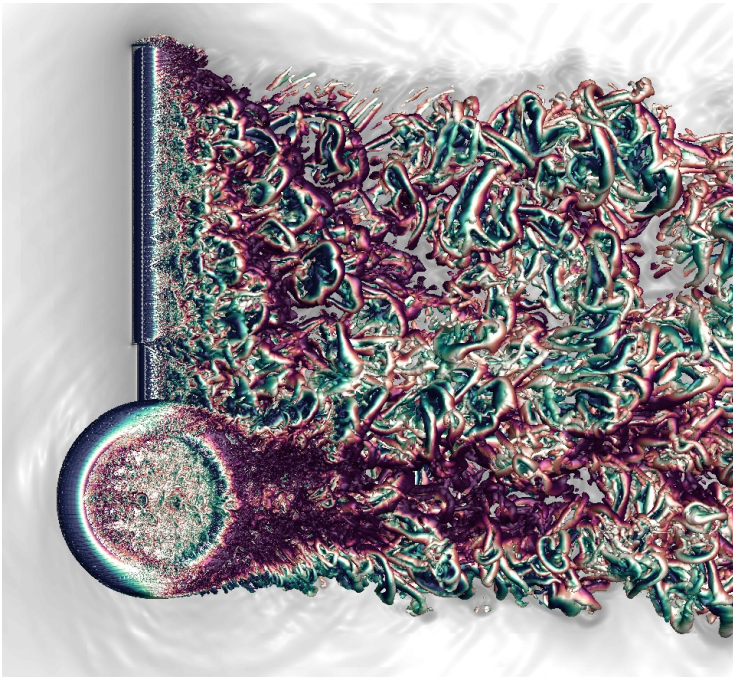
- Strong flow unsteadiness and turbulent eddies shed from the landing gear can be visualized from the iso-surfaces of Q-criterion (second invariant of the velocity gradient tensor) colored y-component of velocity
- Density gradient magnitude contours (in gray scale) on the mid-plane display acoustic waves
- Smaller vortices are generated downstream of the vertical tripping lines on the strut when the grid is refined from grids D to F



Grid D [100.5 M]
tripping case (2)



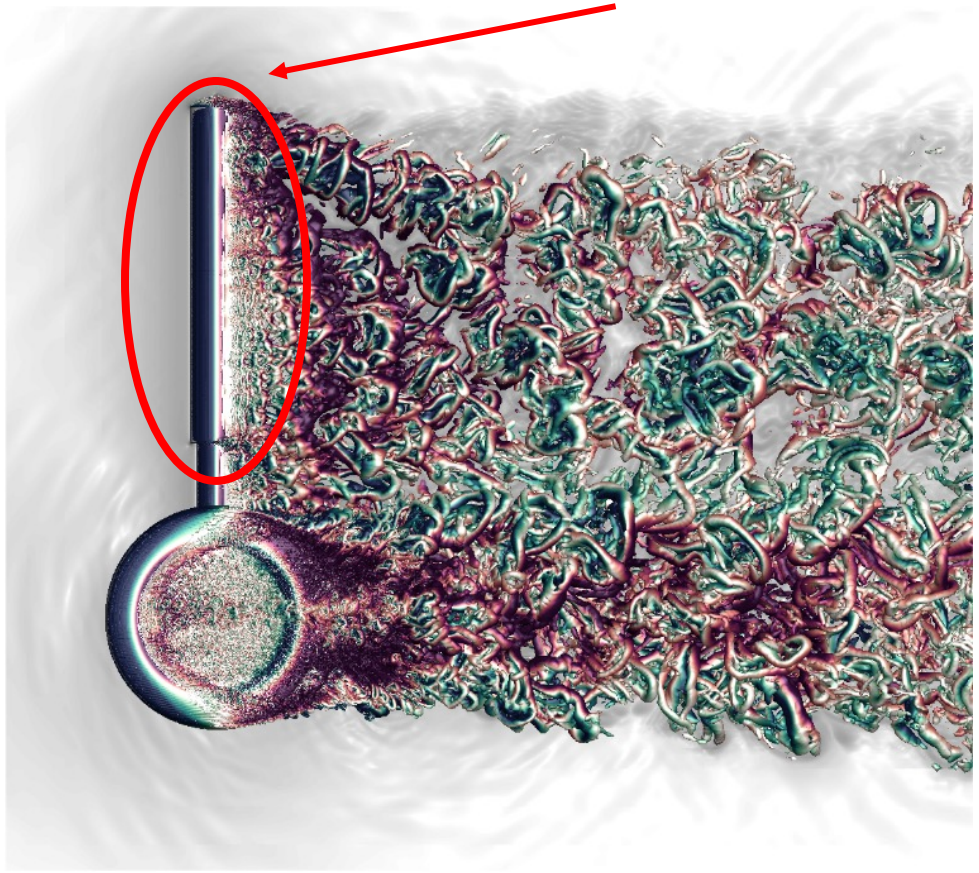
Grid E [309.0 M]
tripping case (2)



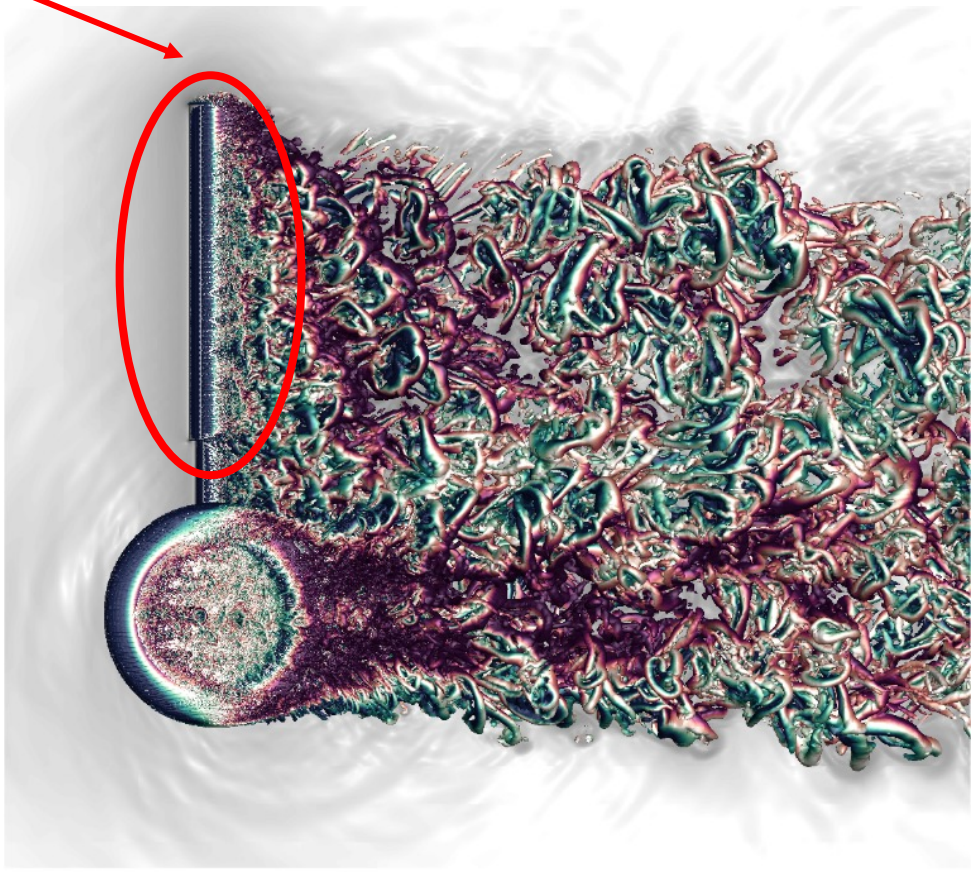
Grid F [737.9 M]
tripping case (2)

Effects of numerical tripping

numerical tripping lines along the main strut help generate more vortices



Grid F **without** tripping



Grid F **with** tripping everywhere [case (2)]

Reynolds numbers of the axle and strut

- Reynolds numbers based on the diameters of axle, lower strut, upper strut are:
  - 2.3×10^5, 2.8×10^5, 3.7×10^5
- These Reynolds numbers fall into the sub-critical and critical ranges of flow past a cylinder
- In these ranges, the wake topology changes drastically with the Reynolds number due to the presence of laminar separation bubbles with combined effects of flow separation, transition to turbulence in the separated regions, and reattachment of the flow
- The tripping devices in the experiments triggered turbulent transition further upstream of the boundary layers

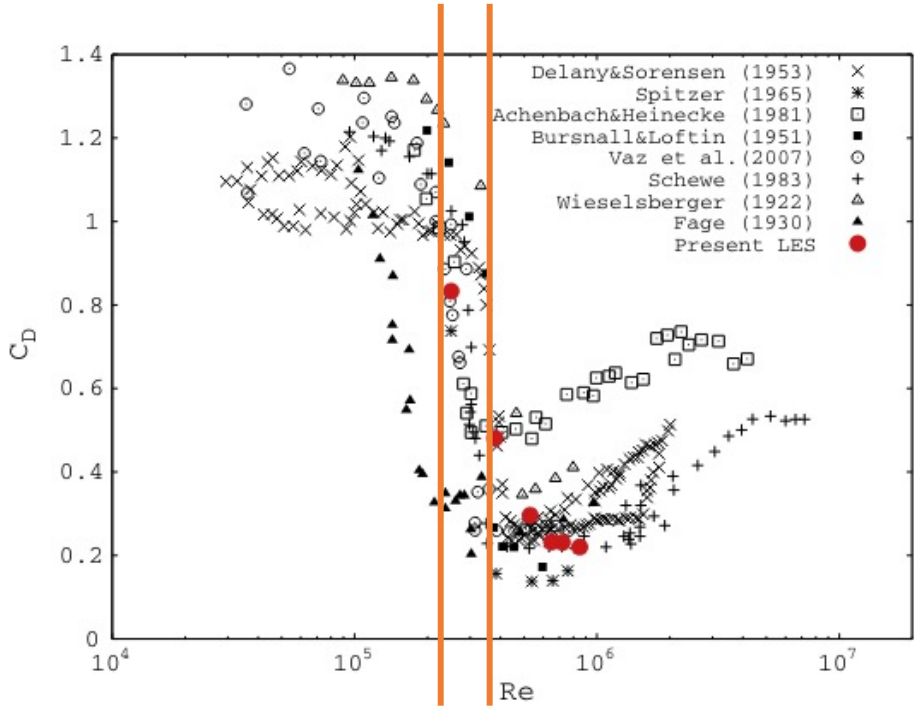


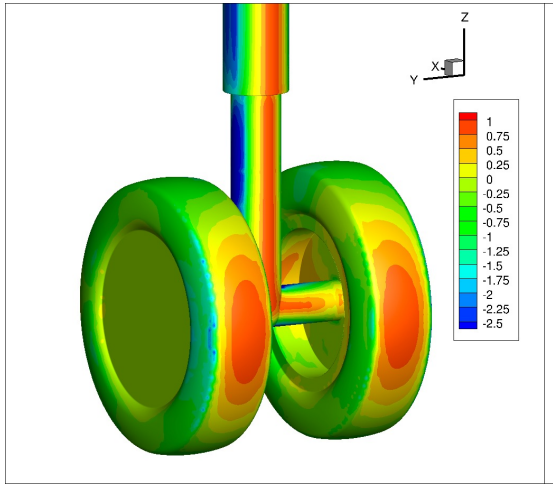
Figure adopted from Rodriguez et al.[1]

1. Rodríguez, I., Lehmkuhl, O., Chiva, J., Borrell, R., and Oliva, A., "On the flow past a circular cylinder from critical to super-critical Reynolds numbers: Wake topology and vortex shedding," International Journal of Heat and Fluid Flow, Vol. 55, 2015, pp. 91–103.

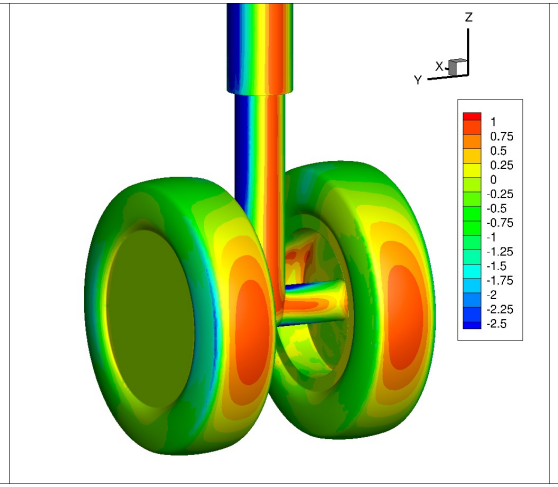
Part I: Near-field Results without Tripping

Mean Wall Pressure Coefficients, c_p

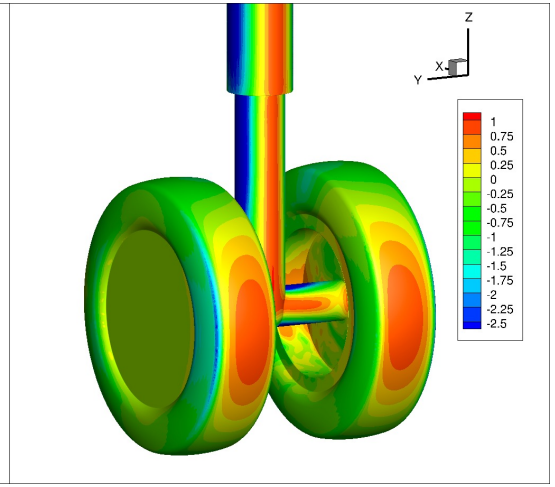
- Surface mean pressure coefficient distributions viewed from upstream are compared
- The c_p on the frontal part and sides of the wheels has small grid sensitivity except grid A due to poor grid resolution
- Grid sensitivities are seen on the sides of the struts



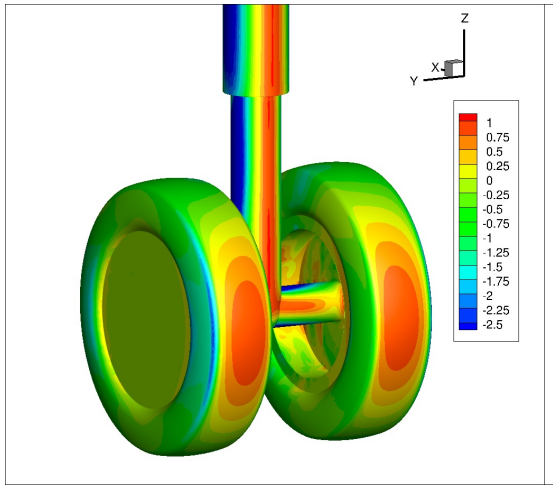
Grid A [2.197 M]



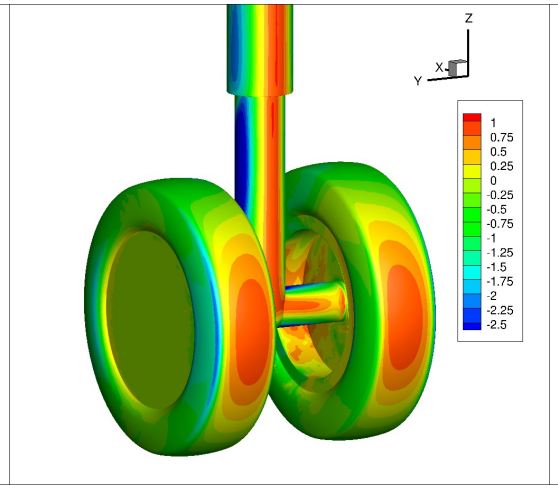
Grid B [6.130 M]



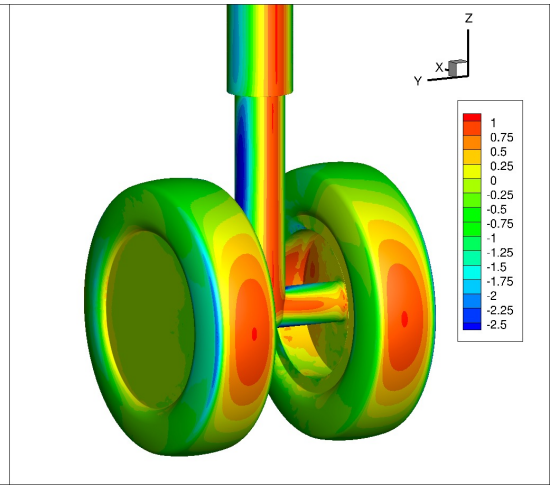
Grid C [22.16 M]



Grid D [100.5 M]



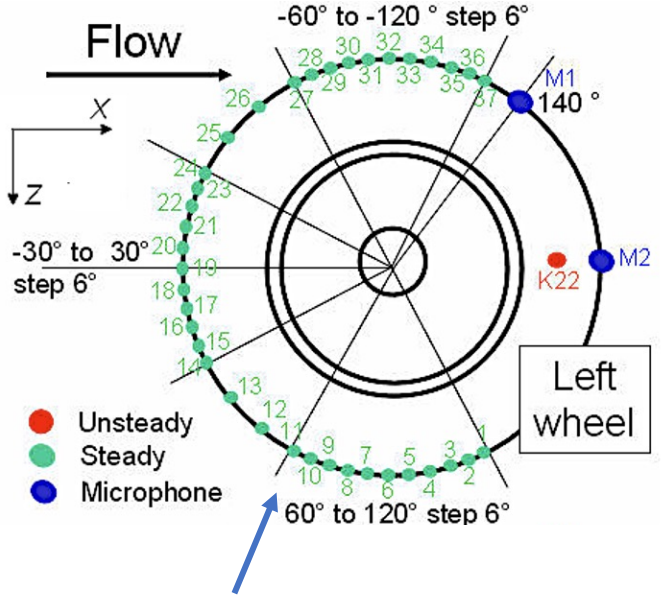
Grid E [309.0 M]



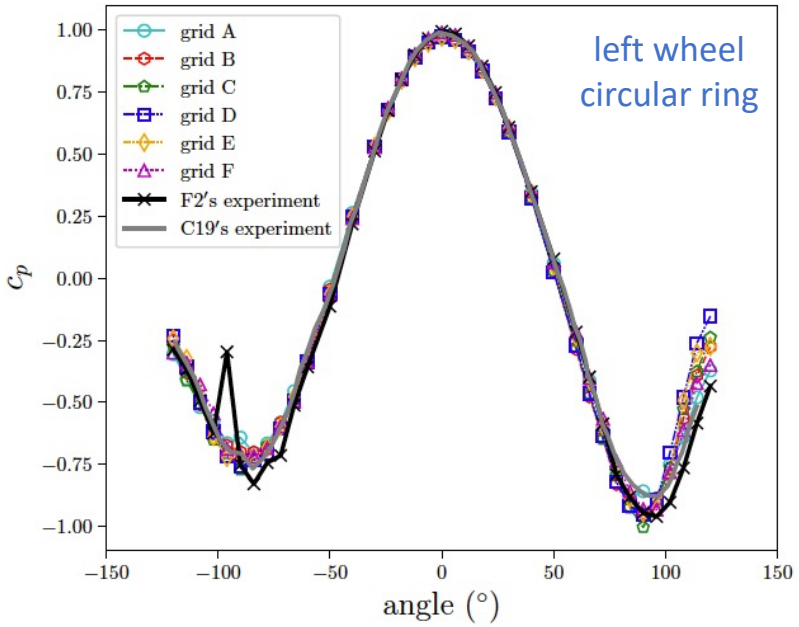
Grid F [737.9 M]

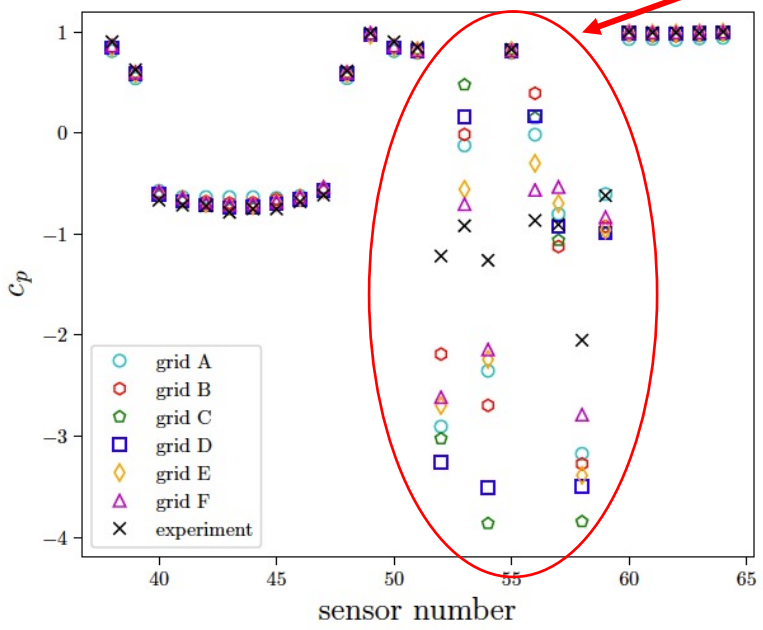
Mean Wall Pressure Coefficients, c_p

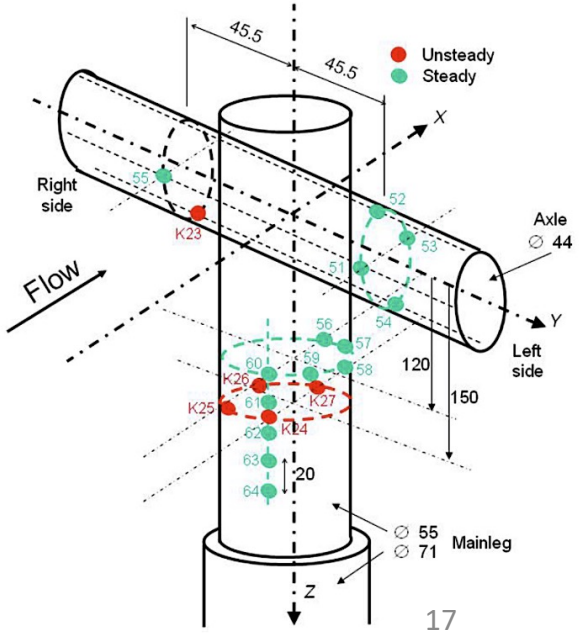
- Small grid sensitivities observed for sensors along the circular ring around the left wheel. Results on wheel agree better with the open wind tunnel (C19) in general
- Large discrepancies are seen for many sensors at axle and strut. Reynolds numbers of axle and strut fall into the subcritical and critical regimes of cylindrical flows. Hence, tripping in experiments has large effect for pressure at these locations which are not modeled in these simulations. The large grid sensitivities are likely originated from the deficiency of wall model for subcritical and critical flows



sensors on axle and strut

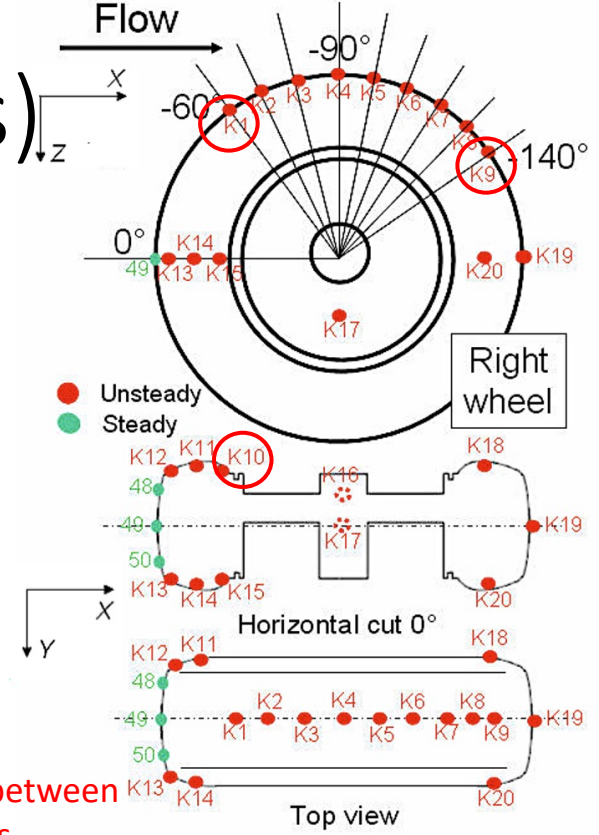




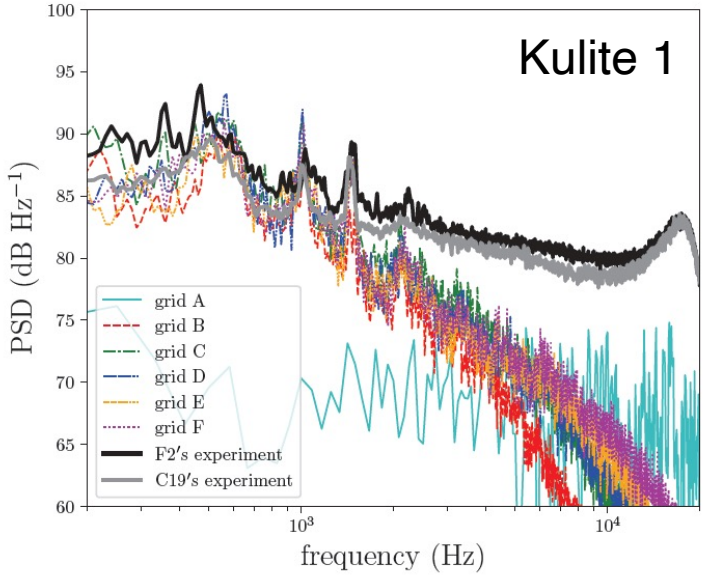


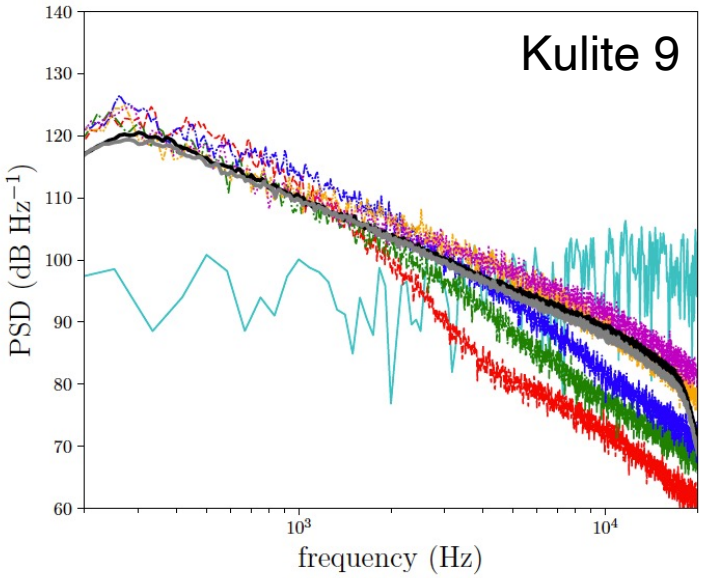
Wall Pressure Power Spectral Densities (PSDs)

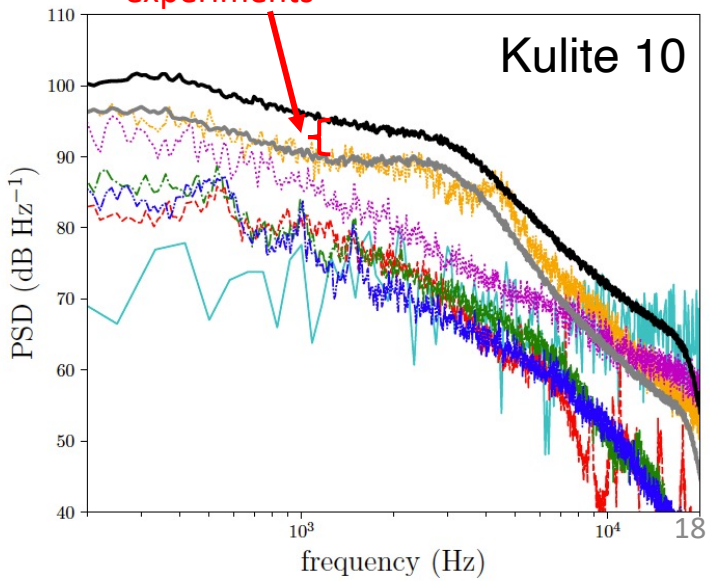
- A physical tripping strip is installed just upstream of Kulite sensor 1 in the experiments and hence there are large under-predictions
- At Kulite 9, the flow has become fully turbulent and is characterized by the broadband noise spectrum. The PSD spectra at this Kulite are accurately predicted with the high resolution grids E and F for almost two decades of frequencies.
- Large grid sensitivity can be seen at Kulite 10. Generally, the PSDs predicted with the high resolution grids are better compared with the experiments, especially for grid E.



large discrepancy between experiments

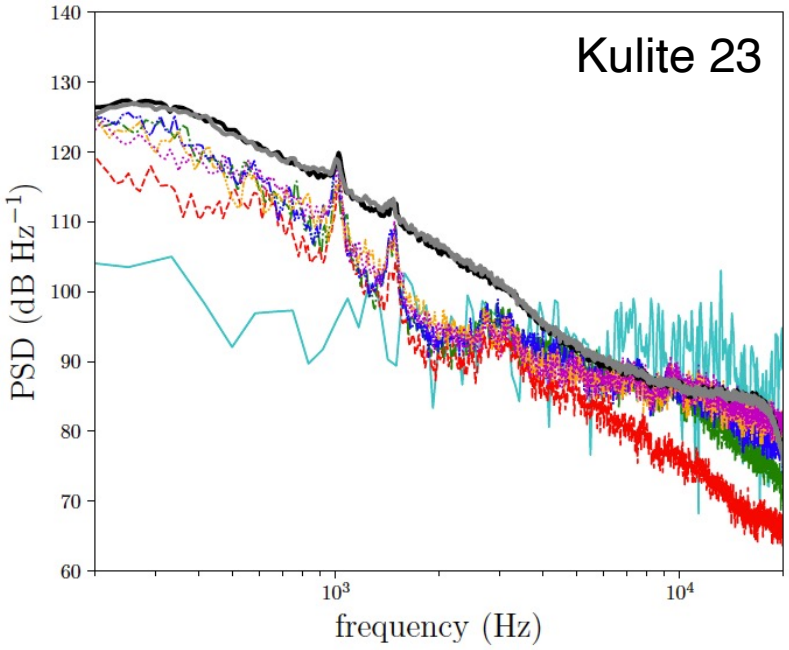


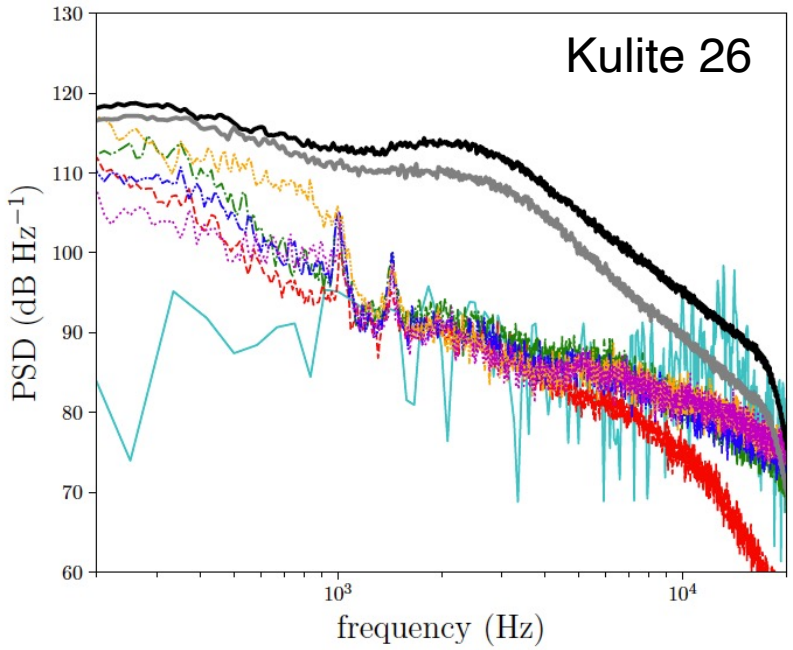


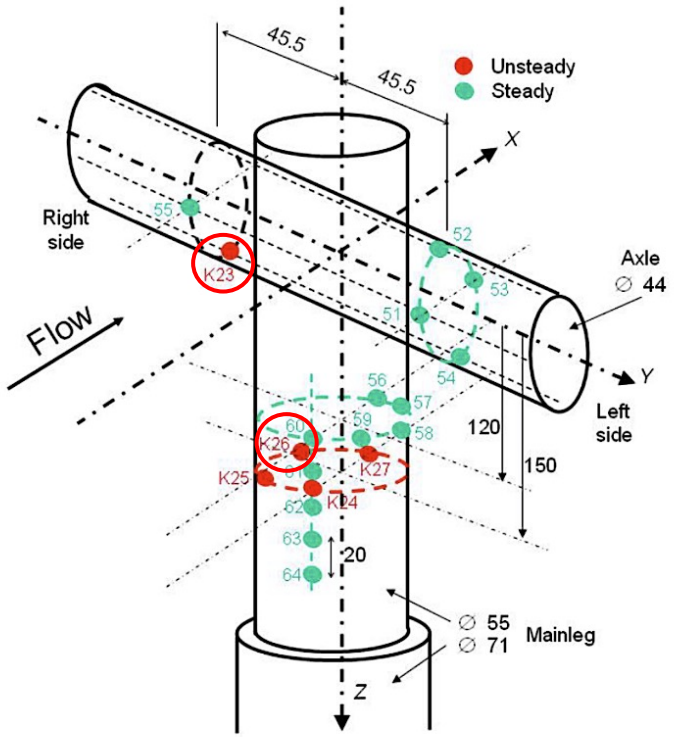


Wall Pressure Power Spectral Densities (PSDs)

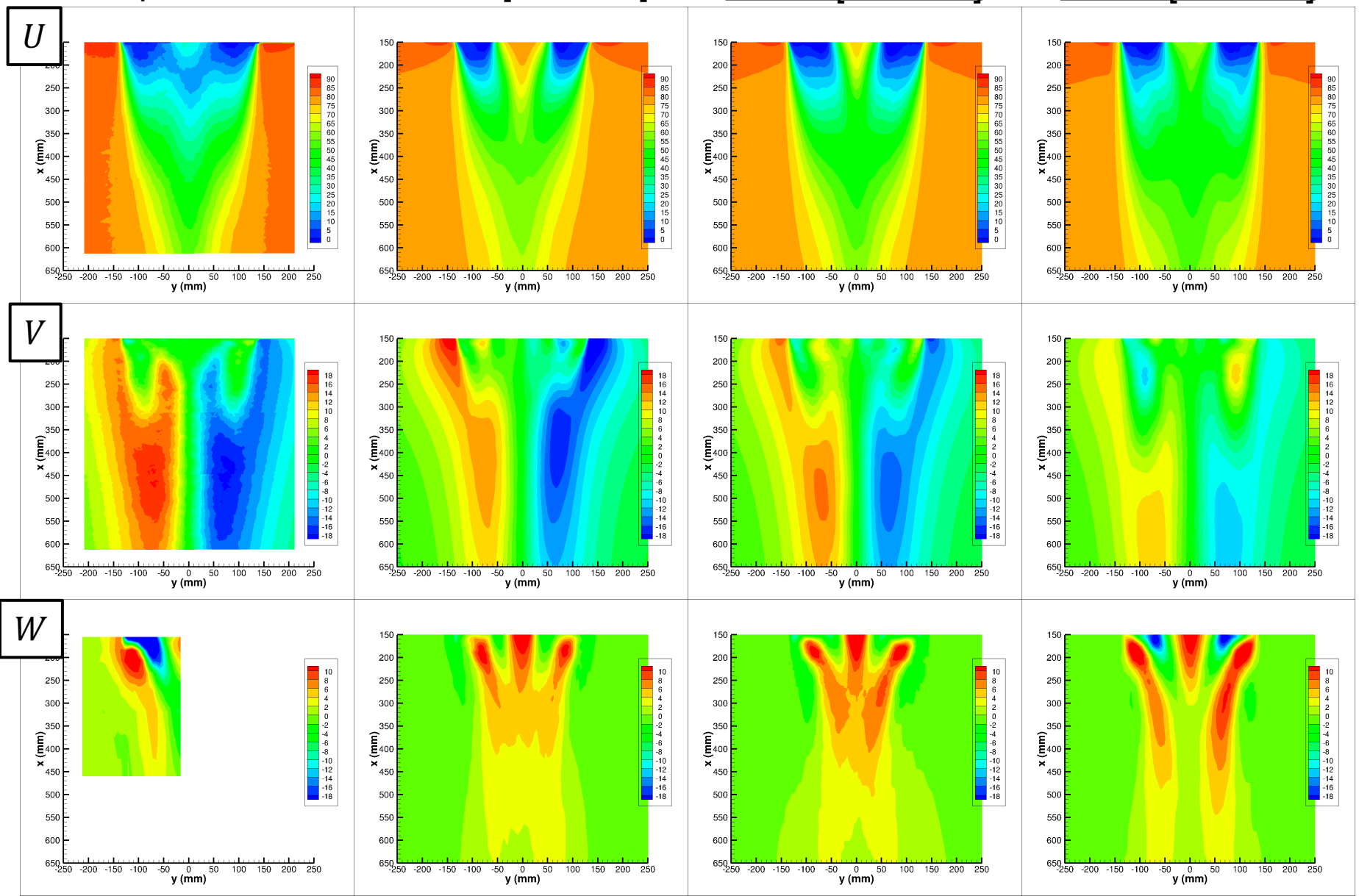
- PSDs at Kulites 23 and 26, which are mounted on the axle and lower leg respectively, are compared
- None of the simulations can predict the spectra well at these two locations because the effects from the tripping dots on the main strut and axle are not modeled in these simulations







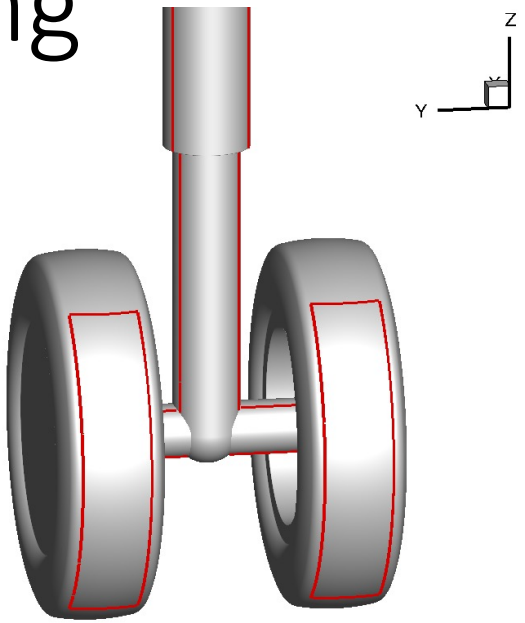
Wake Mean Velocity: Grid Sensitivity



- 2D slices of mean velocity components in the wake region at $z = 0$ (vertical midplane) are compared
- Contours from the simulations are highly symmetric, indicating that a sufficient amount of simulation time is performed
- Over-predictions of U with the simulations in the middle part of the wake near the landing gear, although the over-prediction decreases when the grid is refined
- Large grid sensitivities seen for V and W
- Overall, large discrepancies observed between numerical and experimental results

Part II: Near-field Results with Tripping

case (1): tripping only on axle and main strut
case (2): tripping at all tripping locations in experiments



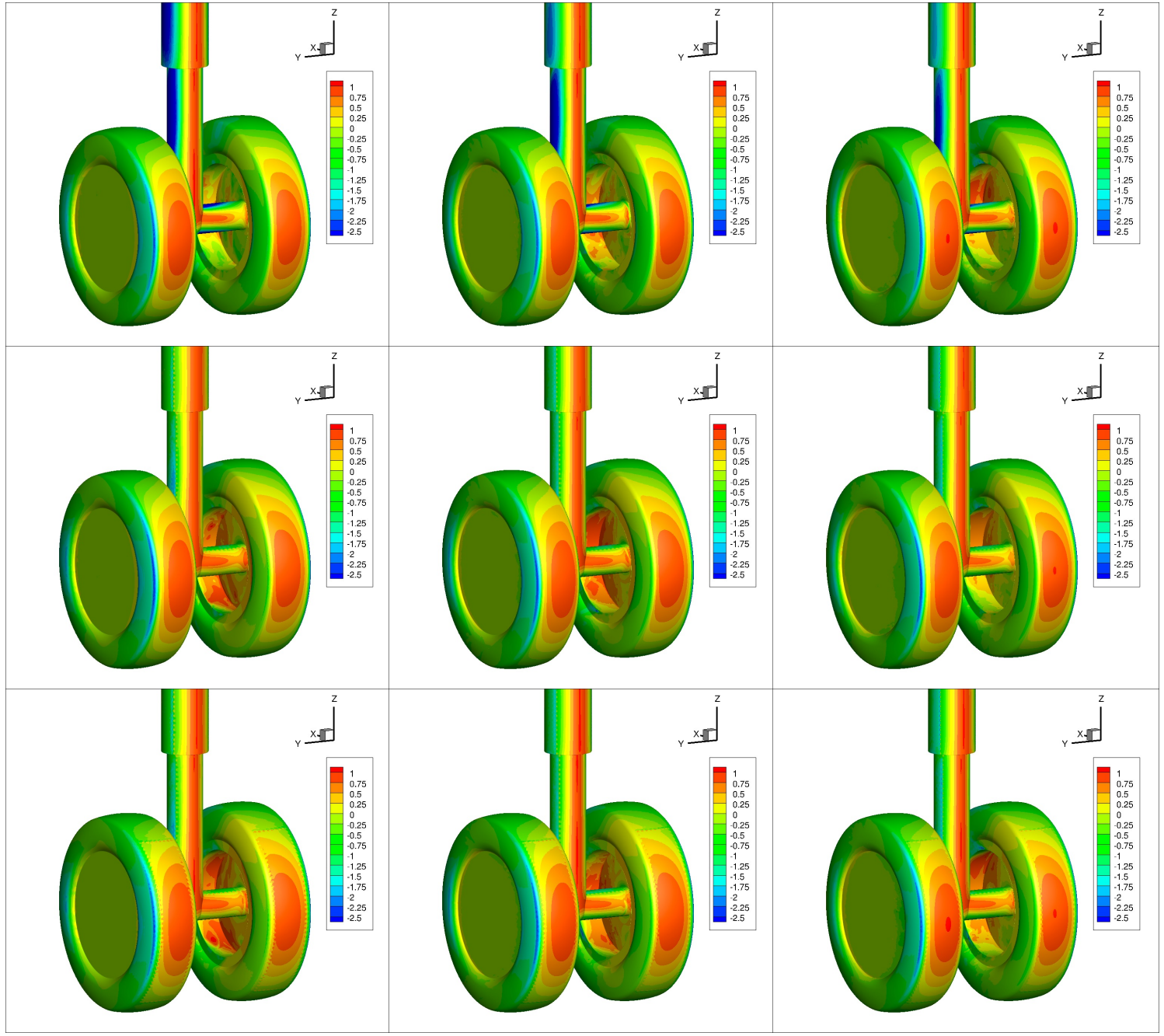
Mean pressure coefficients

- Locations the tripping can be seen in the results obtained with tripping, which appear as dashed lines in the contours of pressure coefficient.
- Insignificant grid sensitivity for the tripping cases for c_p at the frontal parts and sides of the wheels and struts
- The tripping lines on the struts and axle have significant effects on the mean pressure around those components
- The tripping lines on the wheels have small effects on the pressure coefficient contours except in the regions close to those tripping lines

No tripping

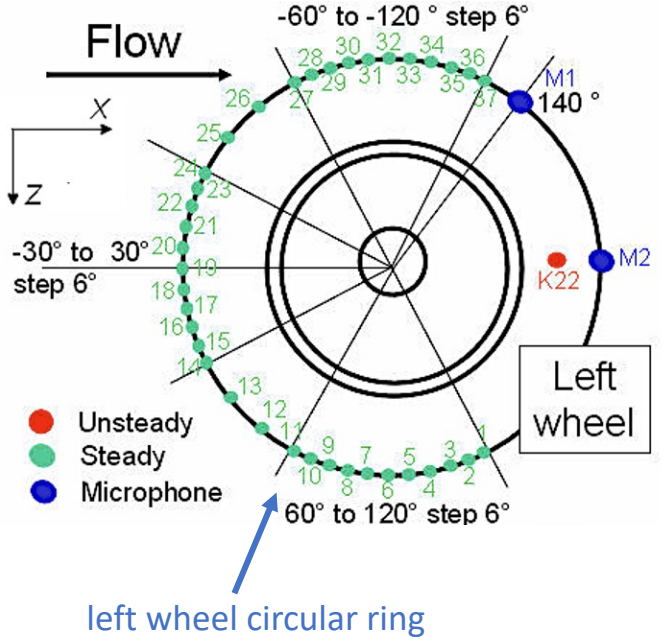
Tripping case (1) on strut and axle only

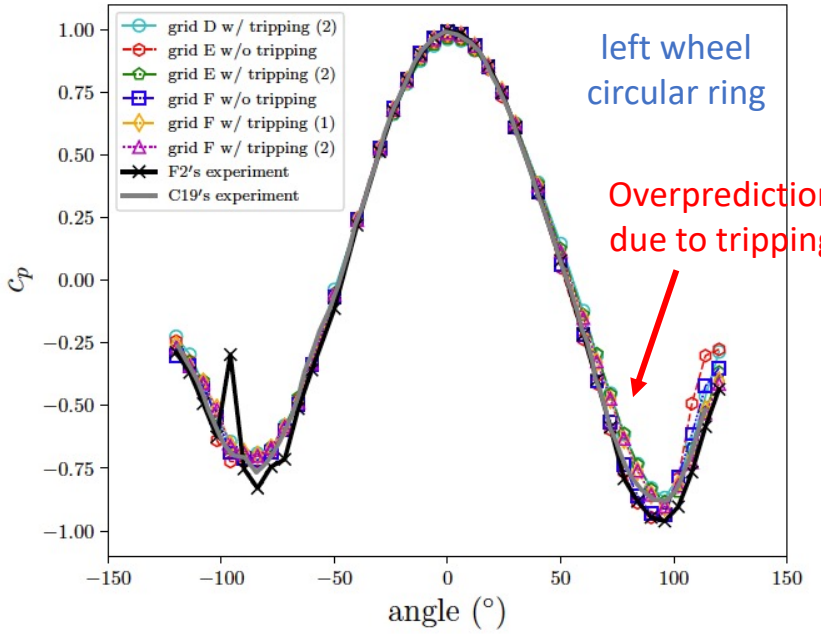
Tripping case (2) everywhere

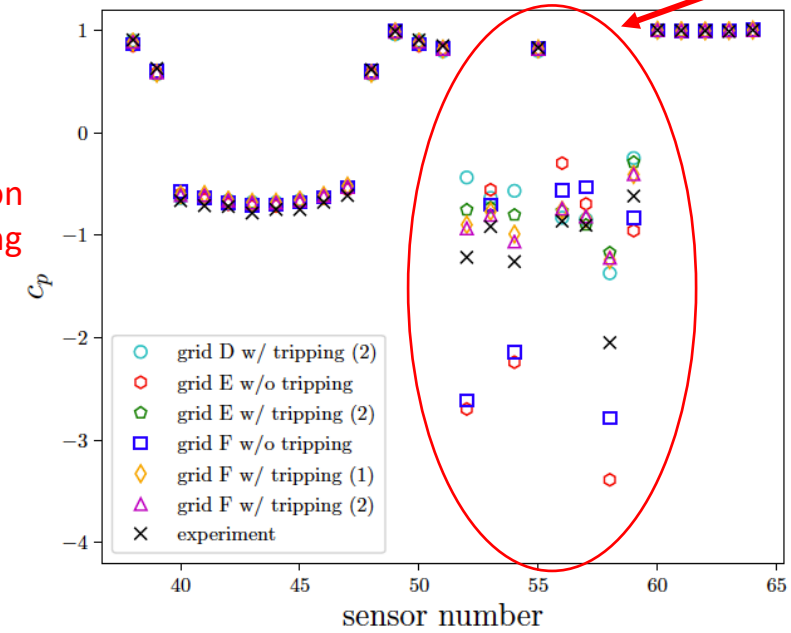


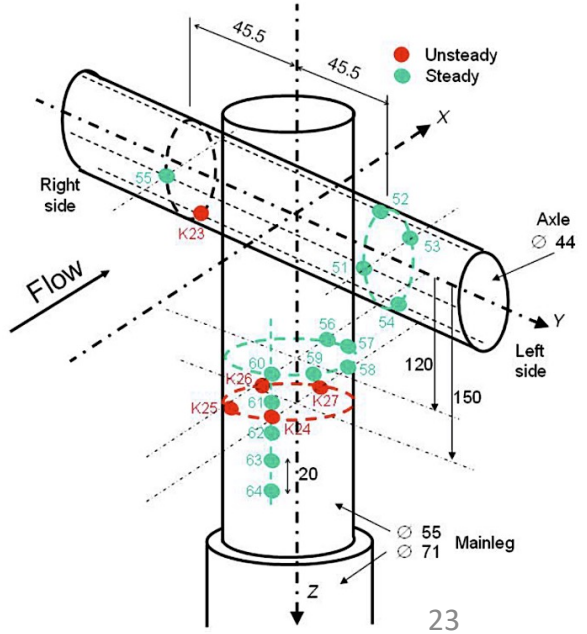
Mean Wall Pressure Coefficients, c_p

- Main effects of tripping are on the top of the wheel and the axle and struts
- The minimum c_p values on the wheel for the tripping cases are closer to the open wind tunnel's (C19) data instead of the closed-loop wind tunnel (F2) since simulations were conducted in an open domain
- Tripping in simulations and experiments triggered turbulent transition further upstream of the boundary layers of axle and strut. Smaller grid sensitivities seen for c_p around the axle and strut. There are better agreements between the simulations and experiments at those locations



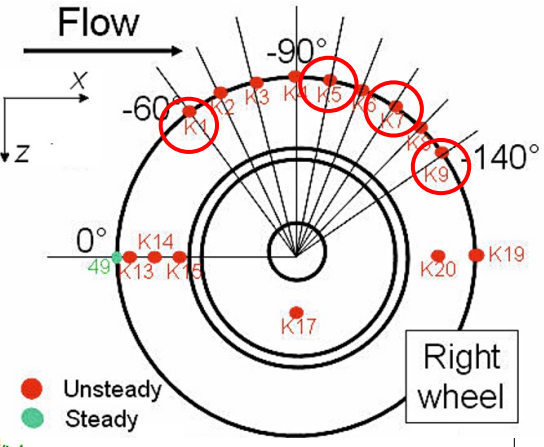


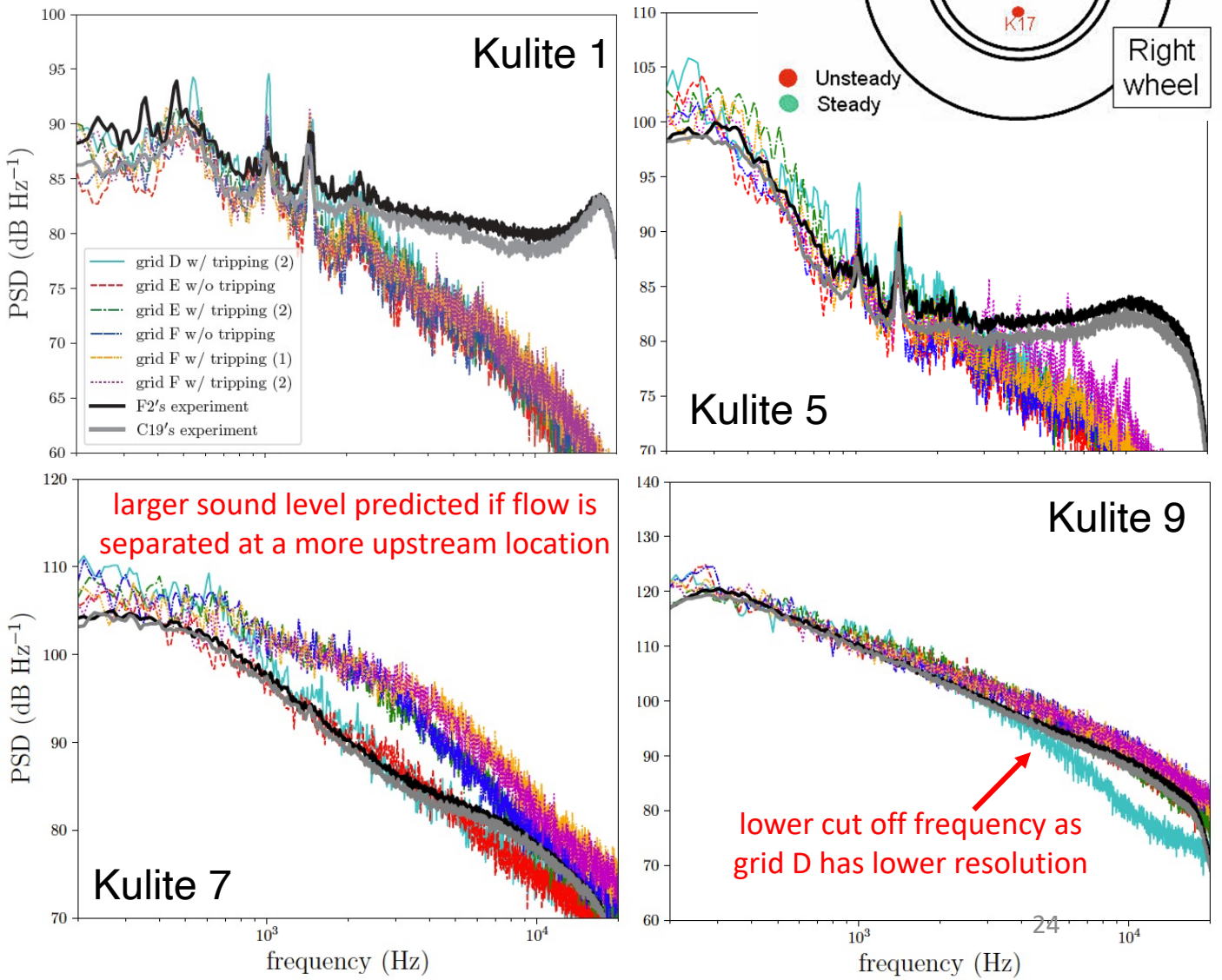




Wall Pressure Power Spectral Densities (PSDs)

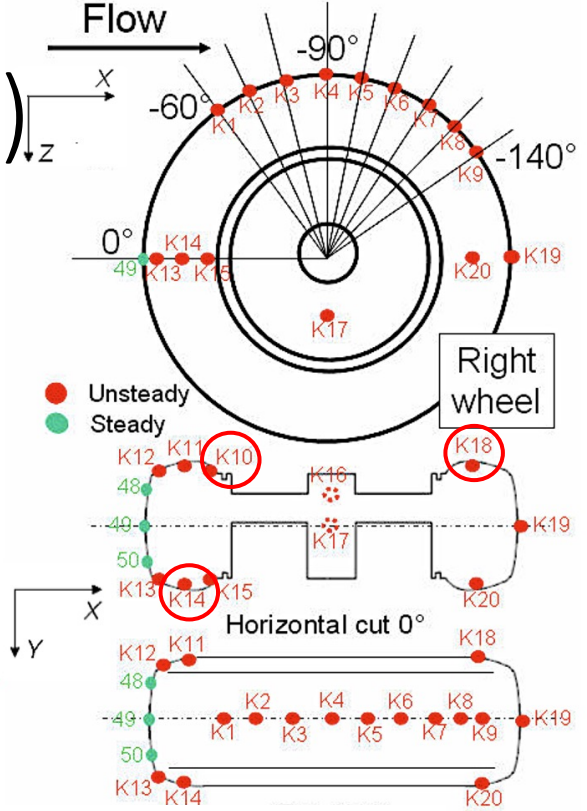
- No influence of the numerical tripping on Kulite 1 that is located right downstream of a tripping strip on the wheel
- High frequency noise at Kulite 5 is excited to slightly higher sound levels for highest resolution grid F by tripping on wheel despite still quite large under-prediction in high frequency range
- The tripping effects in the experiments are challenging to reproduce due to the uncertainties of the small spatio-temporal scales involved
- Kulite 7 is close to flow separation point and the spectra are quite sensitive to grid and tripping mainly from the strut and axle (not wheel)
- Tripping has insignificant effect at Kulite 9 where boundary layer is fully turbulent. Main effect is from grid resolution

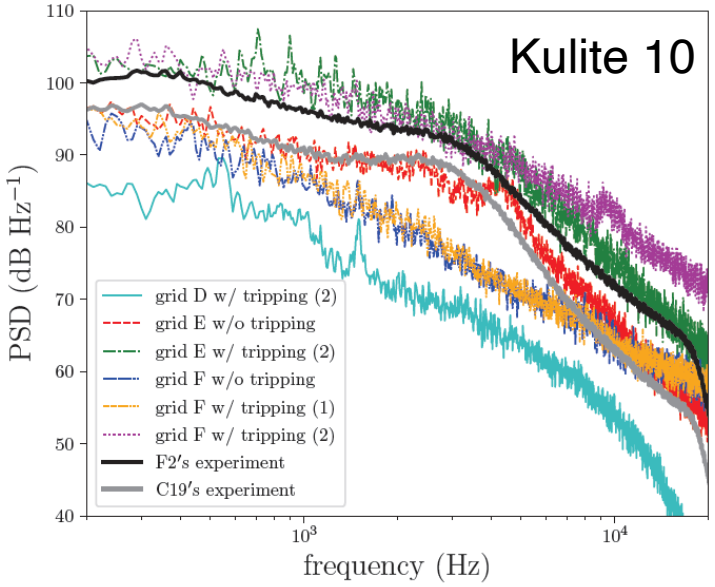


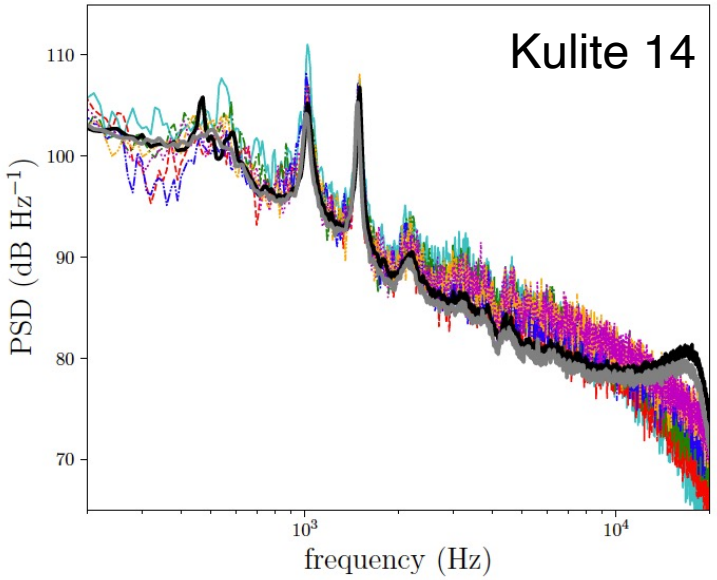


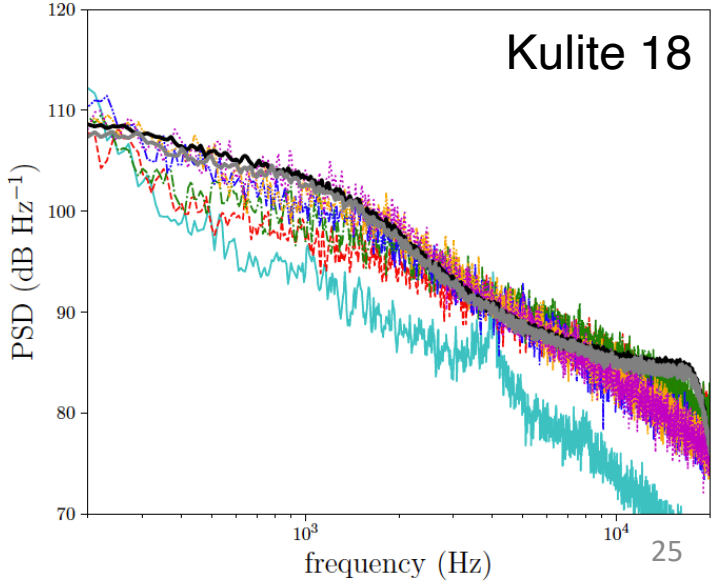
Wall Pressure Power Spectral Densities (PSDs)

- PSDs at Kulite 10 located on the external side are sensitive to the tripping and grid resolution. Even experimental measurements also have a quite large mismatch
- At Kulite 14, tones at around 1 kHz and 1.5 kHz due to cavity resonances are accurately captured in all cases. Overall spectra compare well with the experiments, despite some over-predictions of the sound levels in the high frequency range. Numerical tripping has small effects
- At Kulite 18 which are on the rear and external sides, flow should be fully turbulent. PSDs obtained with grid E & F cases compare well with the experimental results. Numerical tripping has no effect on results with grid E & F



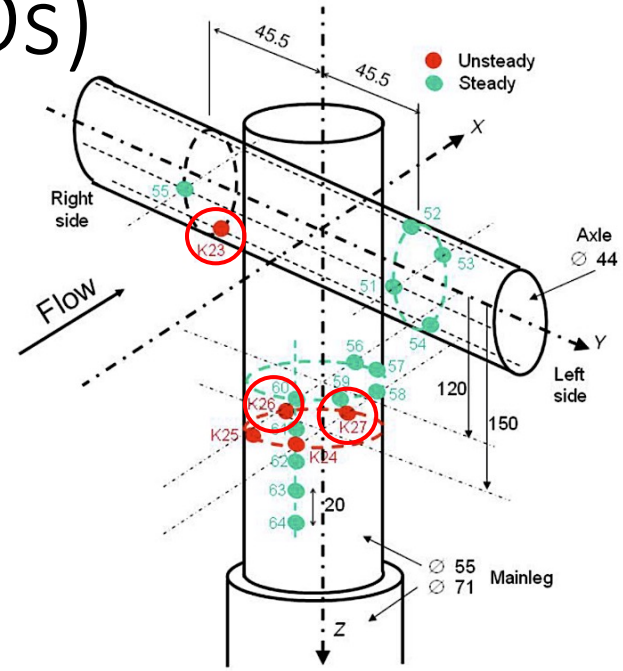


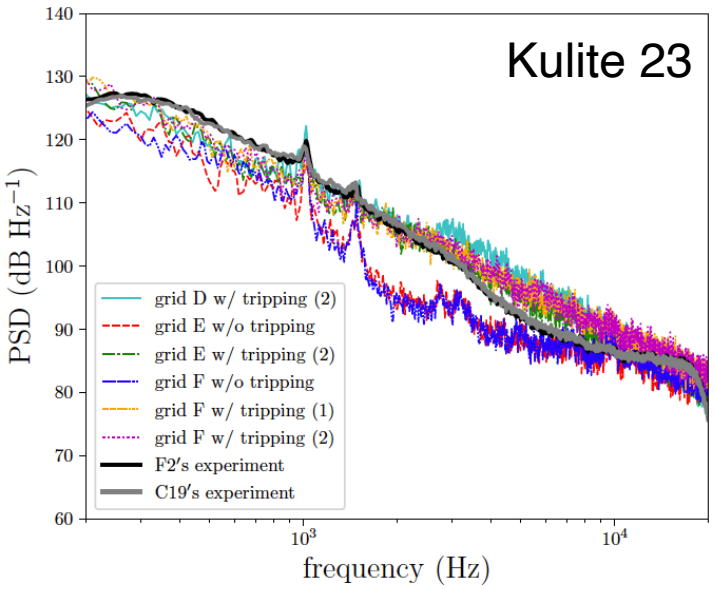


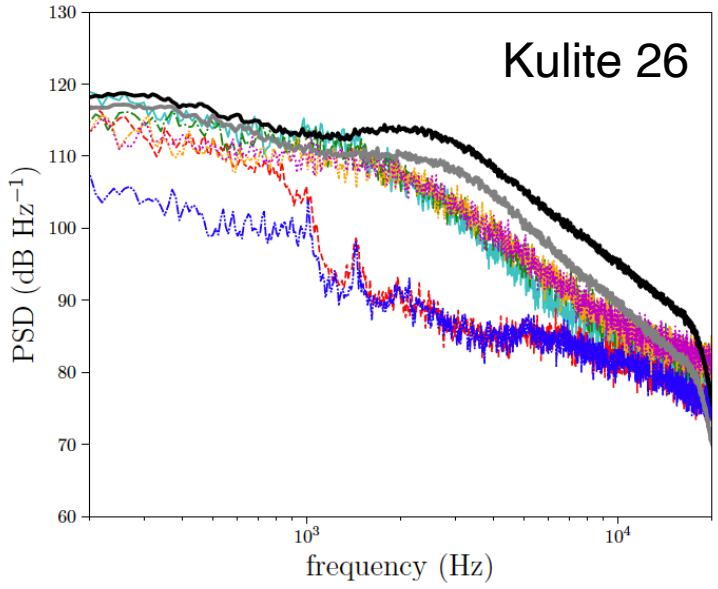


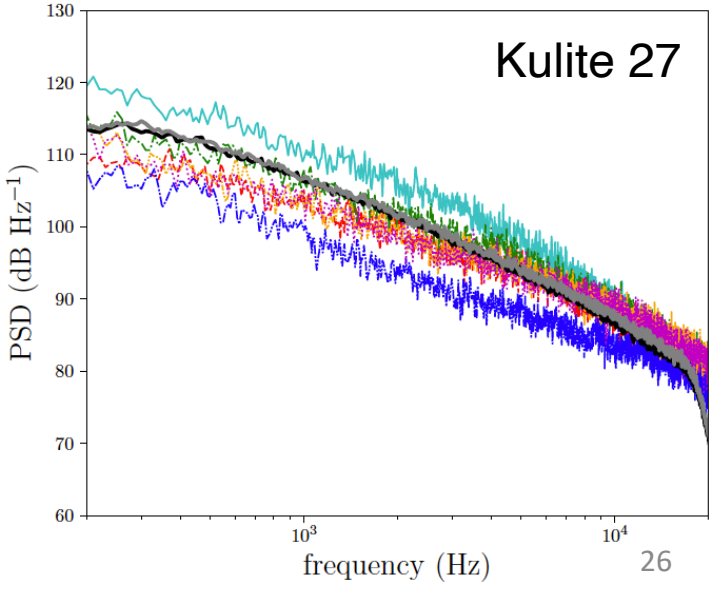
Wall Pressure Power Spectral Densities (PSDs)

- Improvements with the numerical tripping strips are tremendous at some of the Kulites locations on the axle and strut
- PSDs at Kulites 23 and 26, which are on the axle and the lower leg respectively, agree much better with the experimental results. The results with tripping are not quite sensitive to grid resolution. This suggests our numerical tripping model is consistent with grid refinement. More details on tripping settings can be found in the conference paper
- The numerical tripping also improves PSDs predicted by simulations with different grids generally at Kulite 27, where the flow has become fully turbulent





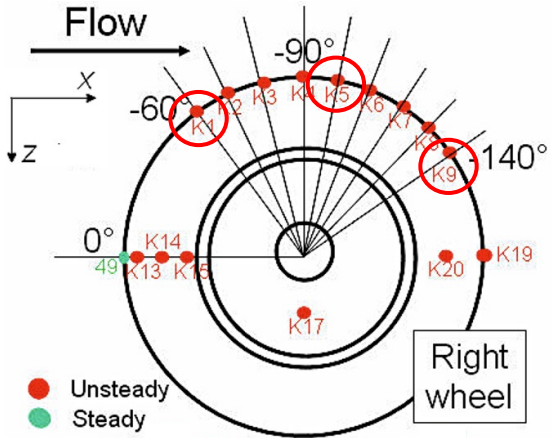




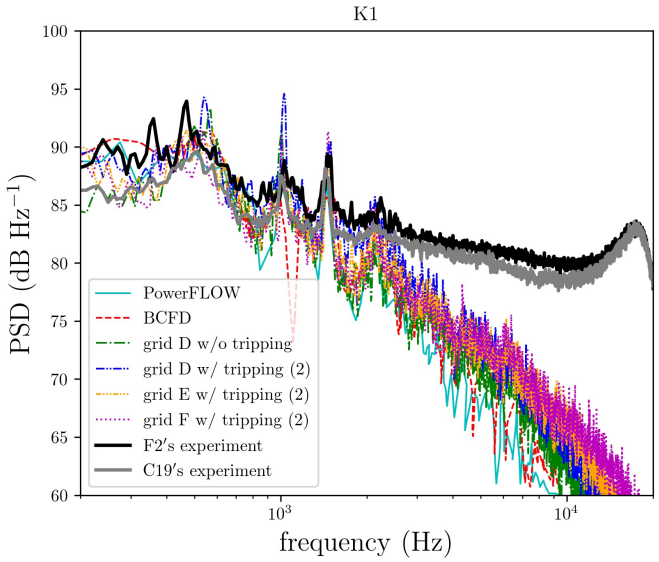
Comparison with the literature

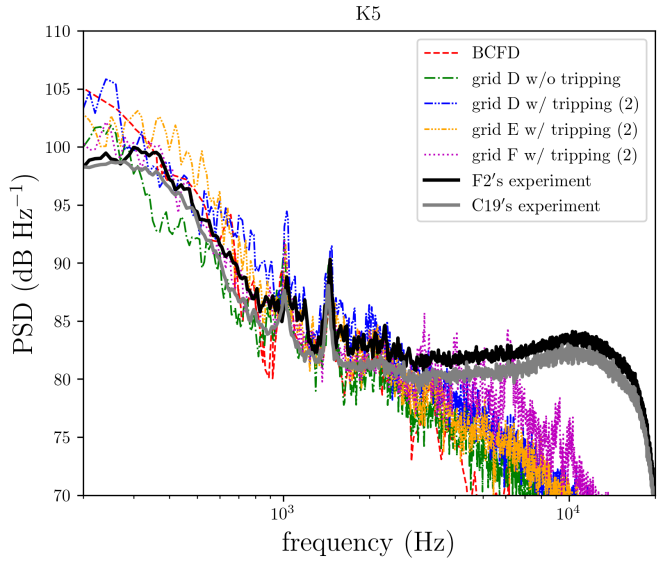
- The near-field PSD results are compared with results from two different papers using hybrid RANS/LES turbulence approach and similar number of grid cells as grid D:

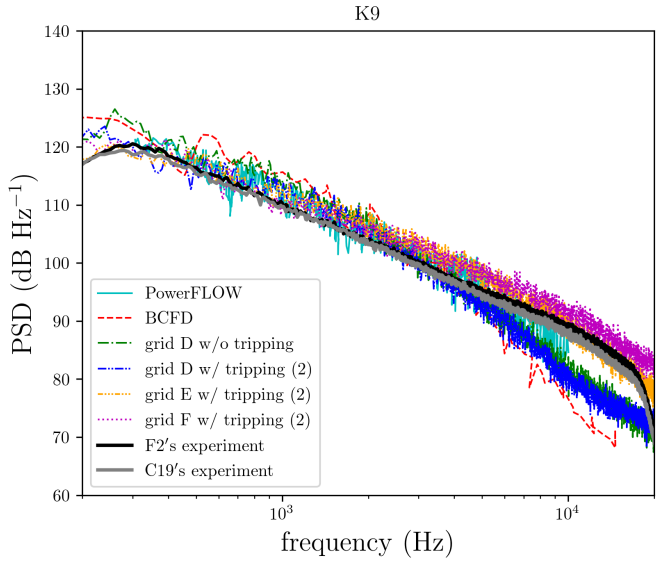
CFD solver	PowerFLOW[1]	Boeing-CFD code (BCFD)[2]	LAVA
Grid paradigm	Octree Cartesian	Unstructured	Octree Cartesian
Numerical method	D3Q19 lattice-Boltzmann with BGK collision operator	2nd order HLLE scheme with a bounded central differencing approach; implicit dual time stepping	4th midpoint-and-node finite difference with HLLC for convective terms; 2nd order for viscous terms; TVD-RK3 time stepping
Turbulence closure	VLES (RNG k-epsilon)	DES (Spalart-Allmaras)	Algebraic WM with Vreman SGS
Number of grid cells (M)	123	99	100.5 (grid D)
Explicit numerical tripping	Yes	No	Yes / No



- Results of grid D are comparable to other simulation results for Kulites on the wheel periphery



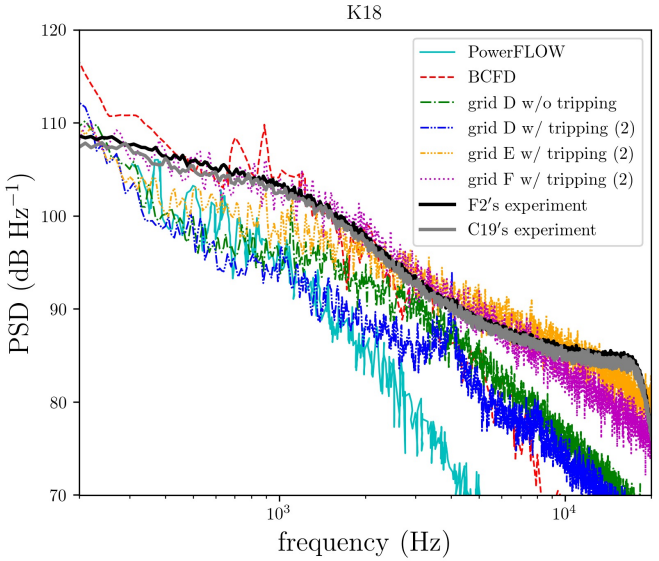


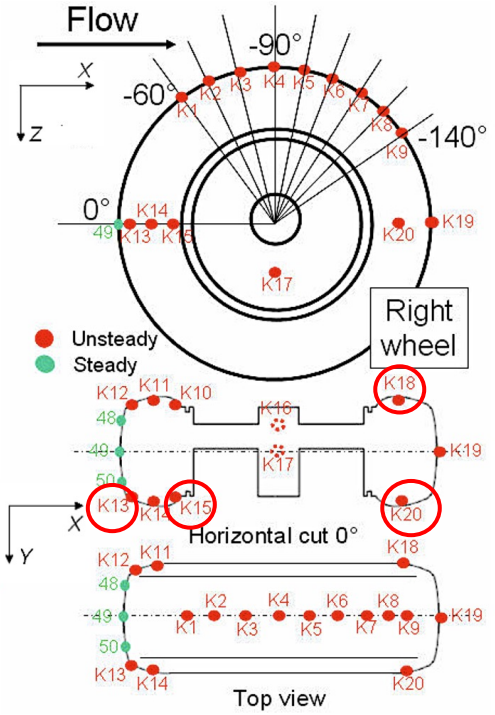


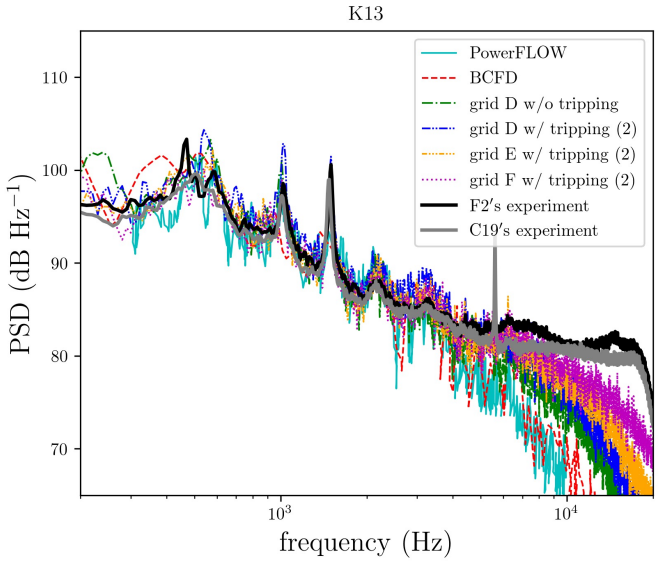
1. Casalino, Damiano, et al. "Lattice–Boltzmann aeroacoustic analysis of the LAGOON landing-gear configuration." *AIAA journal* 52.6 (2014): 1232-1248.
2. Ricciardi, Tulio R., William R. Wolf, and Rachelle Speth. "Acoustic prediction of LAGOON landing gear: cavity noise and coherent structures." *AIAA Journal* 56.11 (2018): 4379-4399.

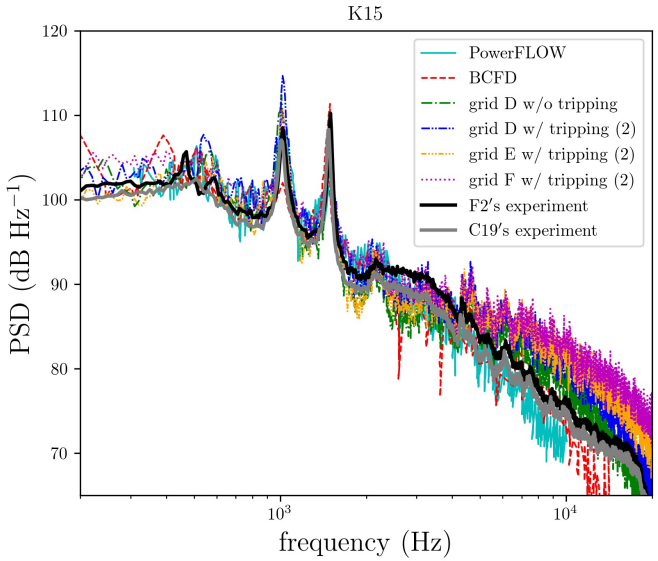
Comparison with the literature

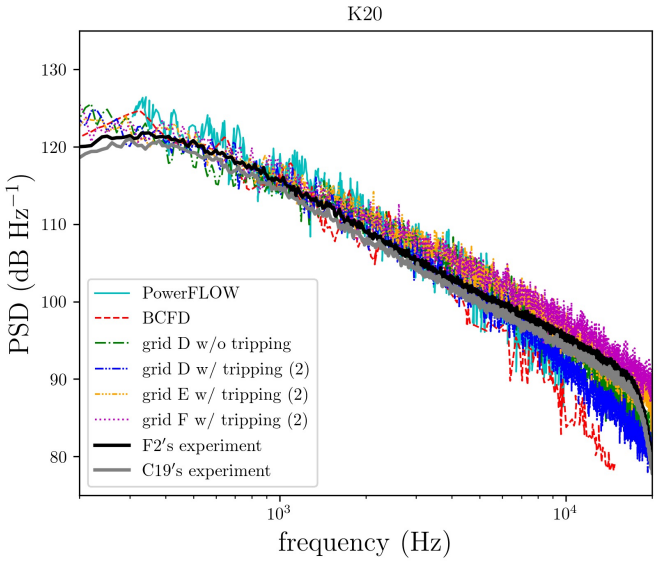
- For the Kulites located on the sides of the wheel, the WMLES results with tripping using grid D are comparable or even better than other literature results, except at K18
- At K18, both the results of grid D and PowerFLOW show under-prediction of the noise level. The PSD is affected adversely by the numerical tripping. Note that numerical tripping is also applied in the simulation of PowerFLOW
- The WMLES results are much improved at K18 with grid refinement





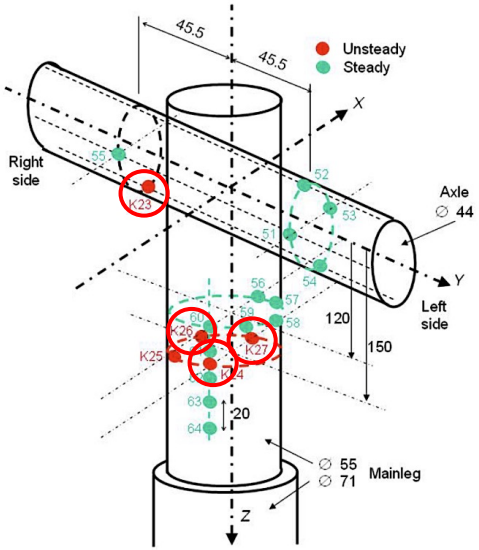


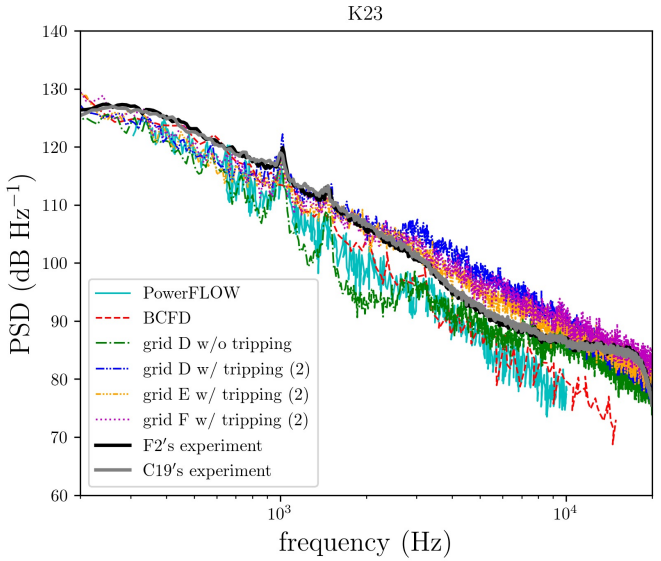


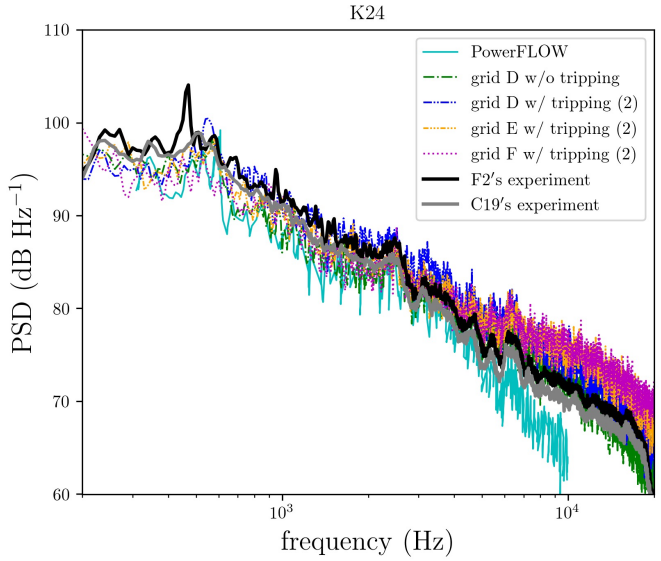


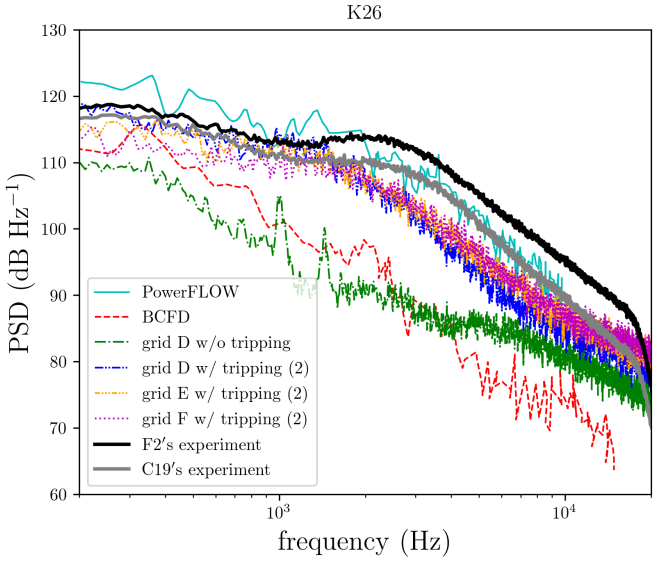
Comparison with the literature

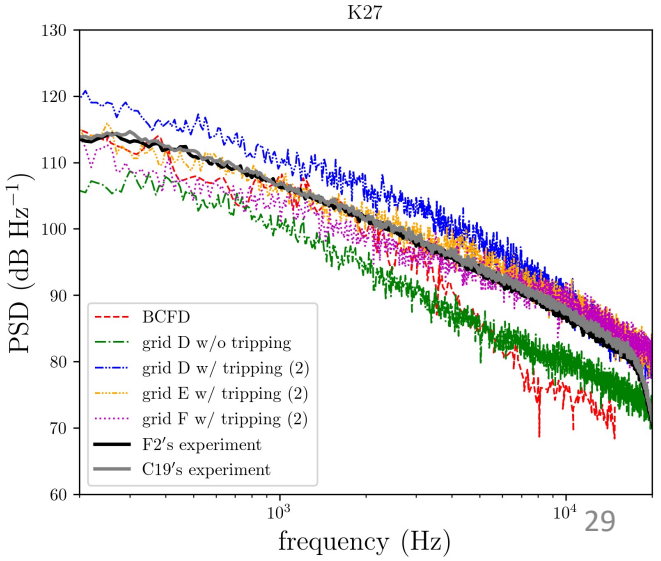
- For the Kulites located on the axle and struts, the WMLES results with tripping using grid D are also comparable or even better than other literature results
- The PSD at K26 is very sensitive with the levels of numerical tripping. The results of BCFD show large under-prediction, similar to our WMLES results without tripping
- At K27, the broadband noise is reasonably predicted with grid D. Results are improved with grid refinement



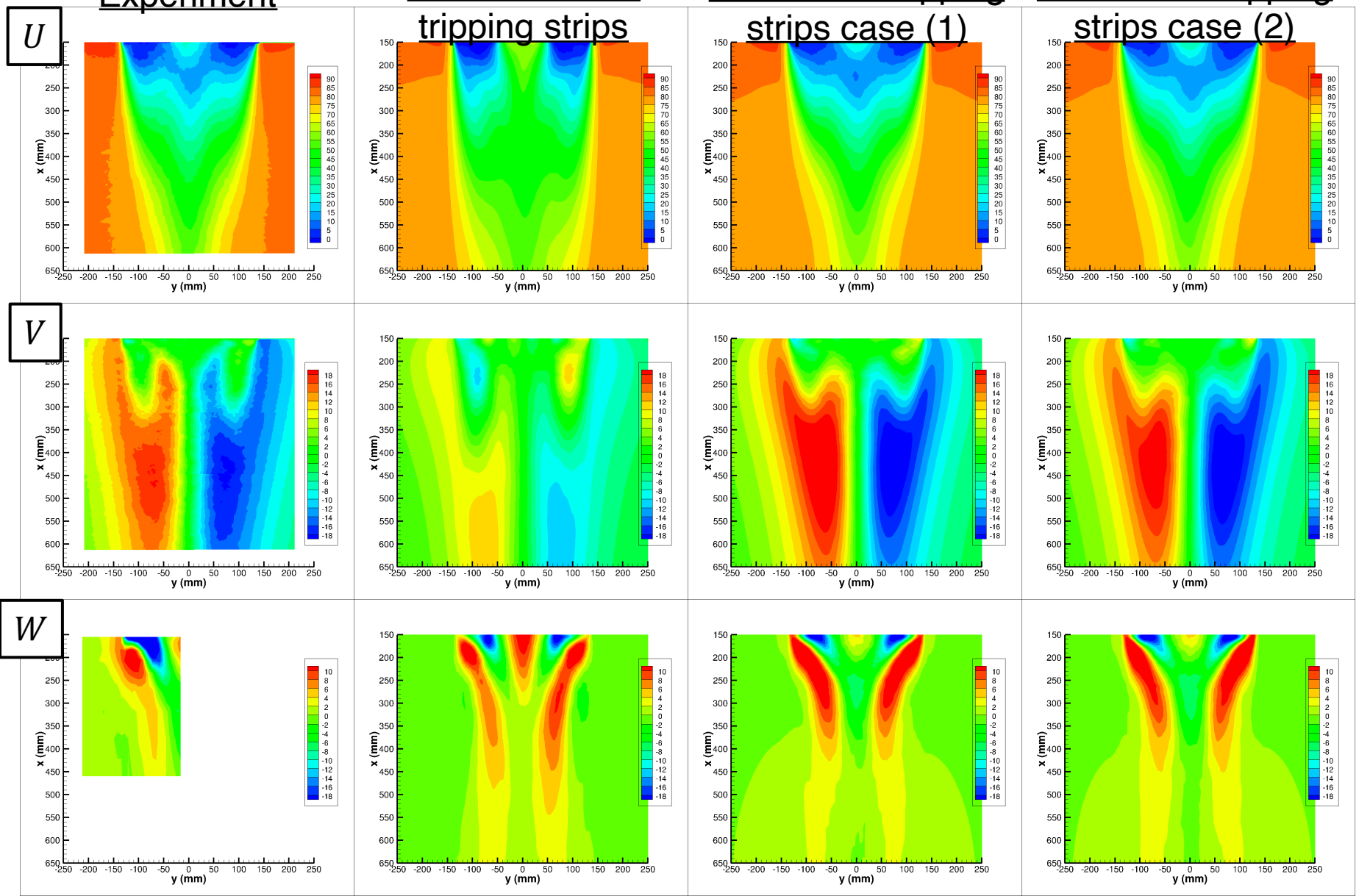






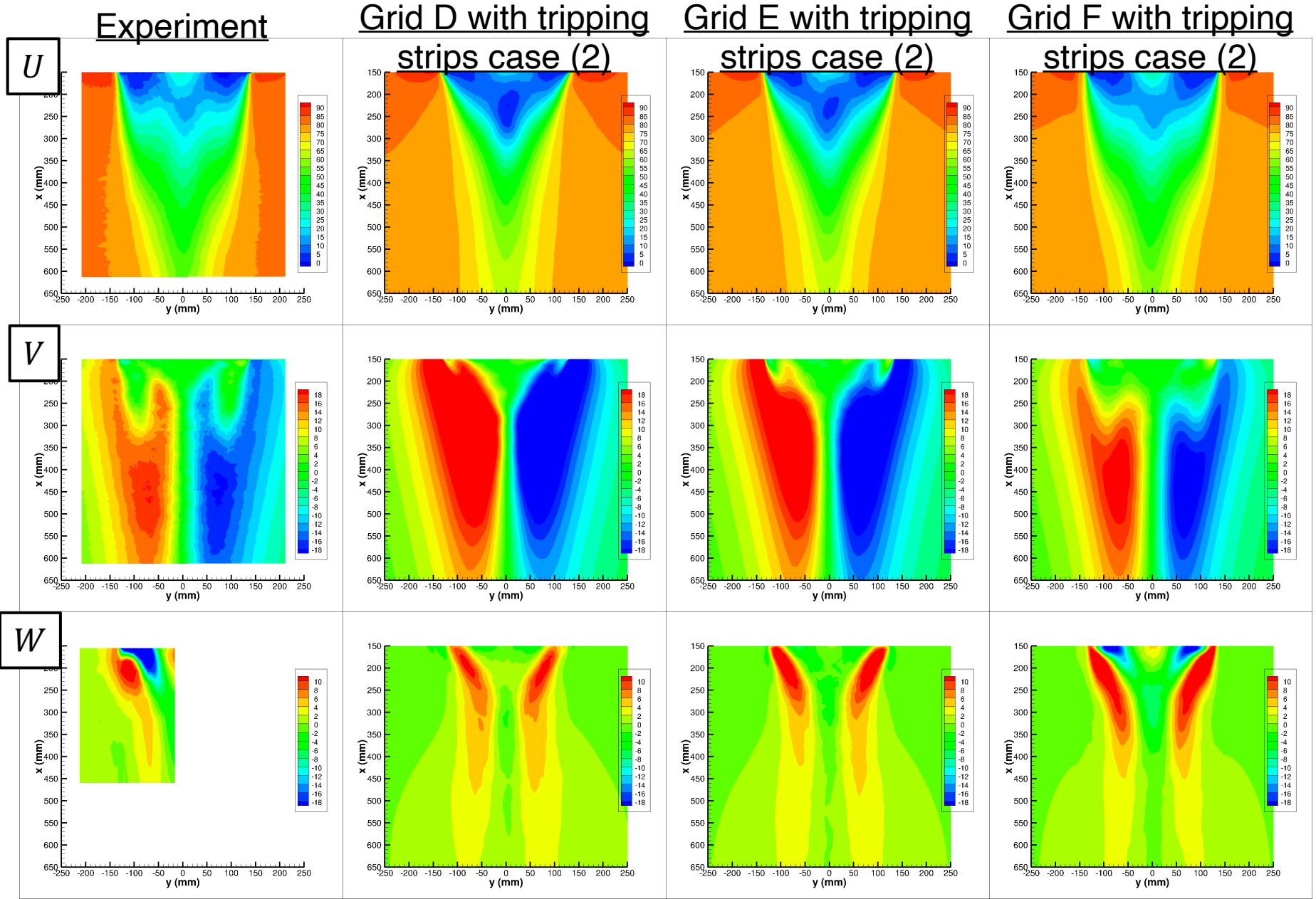


Wake Mean Velocity Fields: Effects of Tripping



- Numerical tripping strips have strong effects on the wake topology and effects mainly come those on the axle and strut
- With numerical tripping, much better predictions of mean velocity profiles from the simulations
- For streamwise U, contours in region around the core of the wake and close to the landing gear are better reproduced with more streamwise momentum deficit
- Magnitudes of transverse velocity component V are also closer to experimental measurements

Wake Mean Velocity Fields with Tripping: Grid Sensitivity

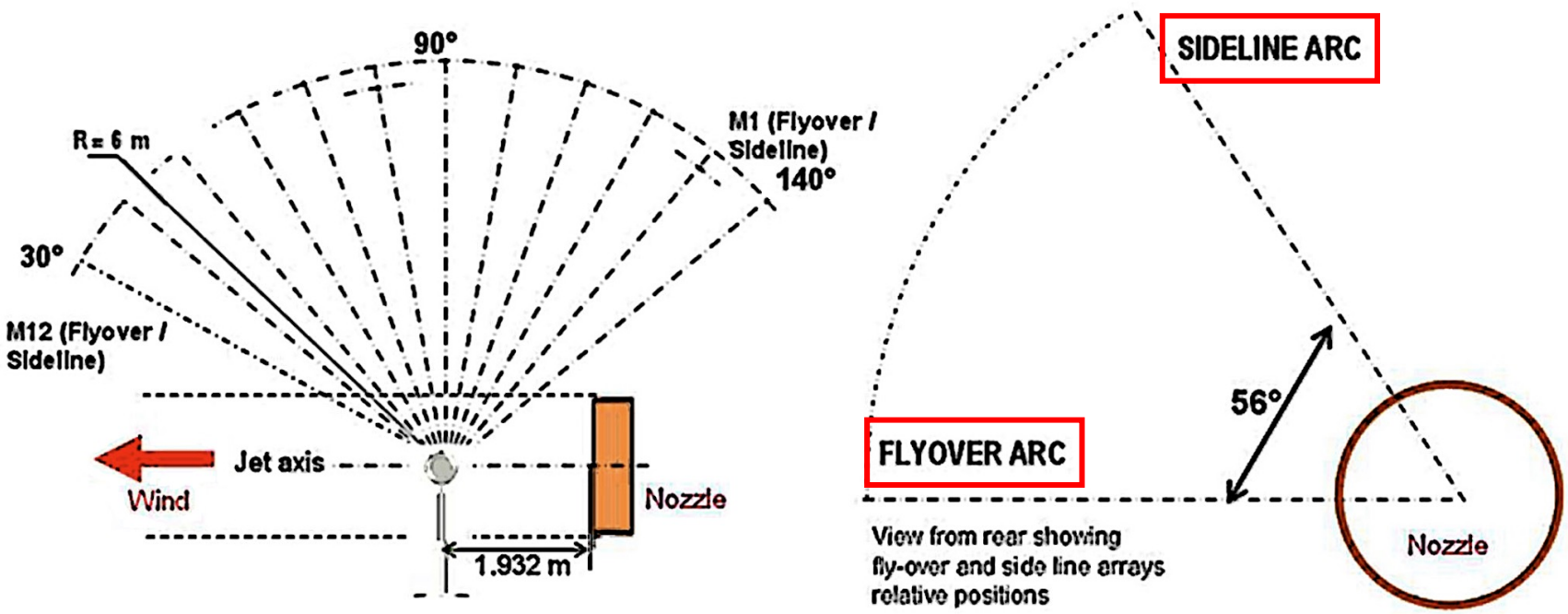


- Simulations with different grids can all capture the low magnitude region of U
- In the middle right downstream of the landing gear, when the grid is refined, there seems to be a trend to converge to the experimental results for all velocity components
- Overall, these results strongly suggest that the modeling of the laminar-turbulent transition induced by the tripping devices on the axle and strut is critical in these WMLESs for reproducing the correct wake topology from the experiments

Part III: Far-Field Acoustic Results

Far-field Acoustics

- The far-field noise was measured in the open jet C19 wind tunnel on two circular arcs located in a flyover plane and a sideline plane respectively with the origin at the landing gear
- 12 microphones are evenly distributed on each of the 2 arcs
- The distance between landing gear and the microphones is roughly $20D = 6$ m



1. Manoha, E., and Caruelle, B., "LAGOON Simplified (2-Wheel) Nose Landing Gear Configuration# 1 Experimental Database," Tech. rep., Technical Report, 2011.

Ffowcs Williams-Hawkings (FWH) acoustic analogy

- The Ffowcs Williams-Hawkings (FWH) equation for a general surface $f(x,t)=0$ in a fluid with quiescent ambient state is given by:

$$\square^2(c_0^2\rho') = \frac{\partial}{\partial t}\left[Q_i\,\hat{n}_i\delta(f)\right] - \frac{\partial}{\partial x_i}\left[L_{ij}\hat{n}_j\delta(f)\right] + \frac{\partial^2}{\partial x_i \partial x_j}\left[T_{ij}H(f)\right],$$

- $\square^2$ is the wave operator, Q_i is the surface mass flux vector, L_{ij} is the surface momentum flux tensor, T_{ij} is the Lighthill stress tensor
- Using the free-space Green's function, the integral solution of the pressure fluctuation p' at far-field is given by:

$$p'(x,t) = \underbrace{p'_T(x,t)}_{\text{thickness noise}} + \underbrace{p'_L(x,t)}_{\text{loading noise}} + \underbrace{p'_Q(x,t)}_{\text{quadrupole noise (ignored)}}$$

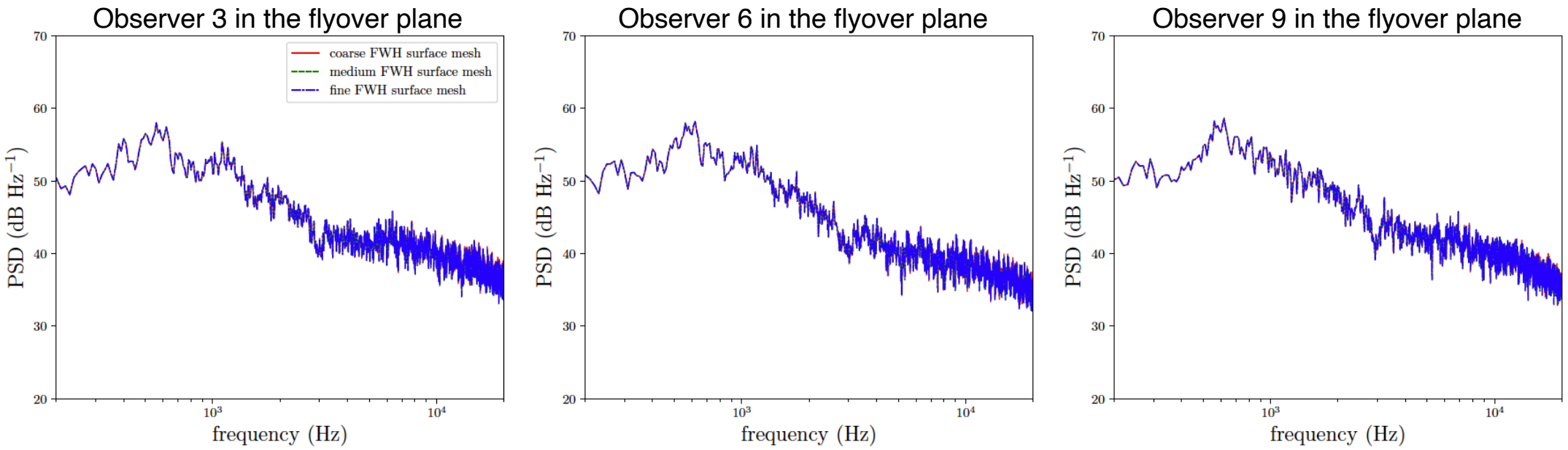
- The **solid (impermeable) FWH approach** with FWH surface placed on the landing gear geometry is adopted in this study since the results obtained with the solid FWH formulation are in general better than those with the permeable FWH approach in the BANC workshop
- The integral forms of the thickness and loading noises are given by the Formulation 1A of Farassat et al.
- Freestream Mach number is set to zero since a large portion of acoustic radiation occurs in quiescent air inside the C19 facility[1]

1. Ricciardi, Tulio R., William R. Wolf, and Rachelle Speth. "Acoustic prediction of LAGOON landing gear: cavity noise and coherent structures." *AIAA Journal* 56.11 (2018): 4379-4399.

FWH Surface Mesh Sensitivity

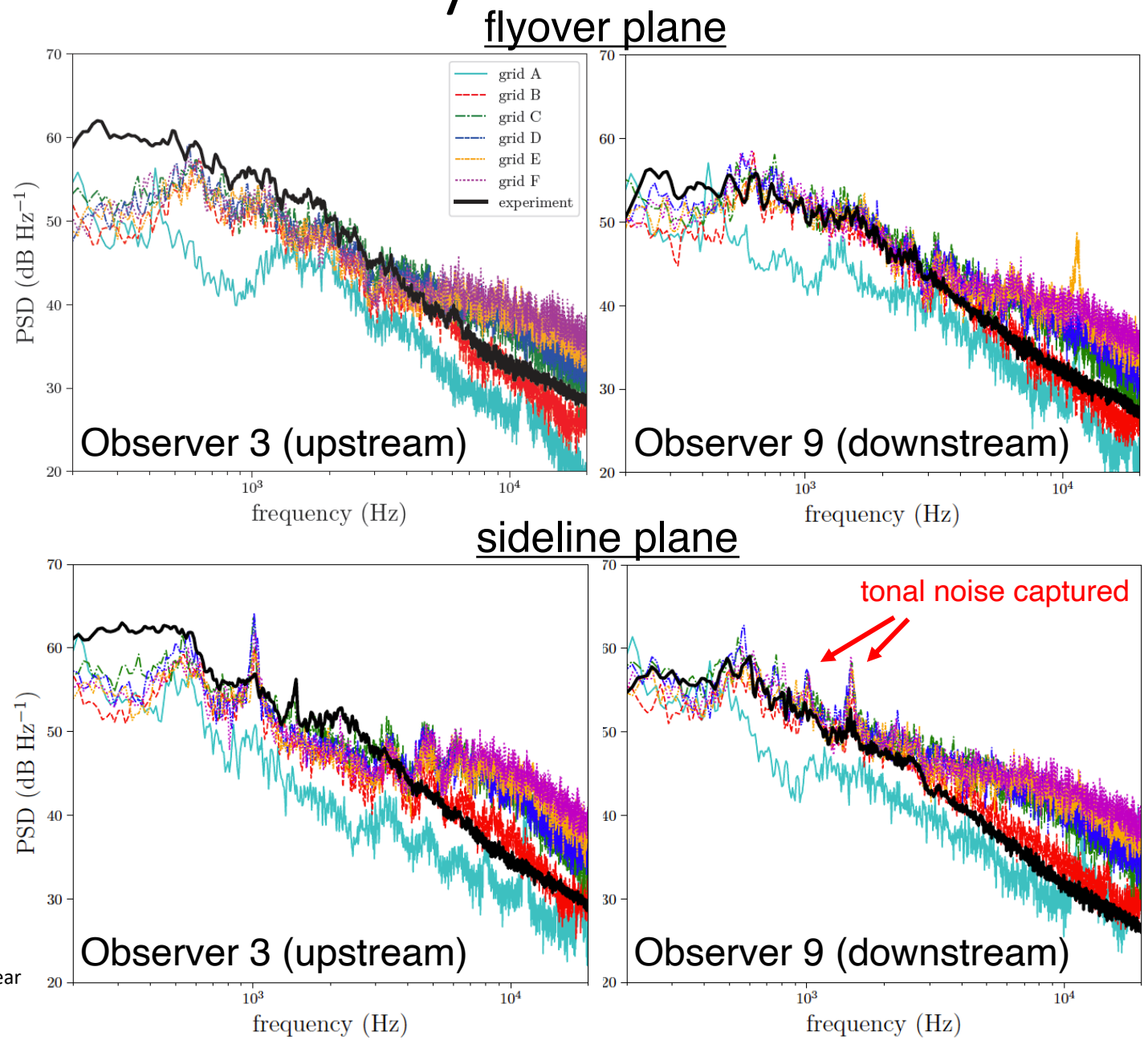
- The surface mesh used for FWH surface can be naively chosen as that used for the immersed boundary method
- Grid sensitivity of FWH surface mesh on the far-field acoustics is investigated with grid F results (without tripping)
- No grid sensitivity is seen from the plot at different observers' locations, indicating lower resolution FWH surface mesh can be used to reduce disk storage

Mesh	Surface element spacing (mm)	Number of surface elements (M)
coarse	2.00	0.360
medium	1.00	1.451
fine	0.50	5.763



Far-field Acoustics: Grid Sensitivity

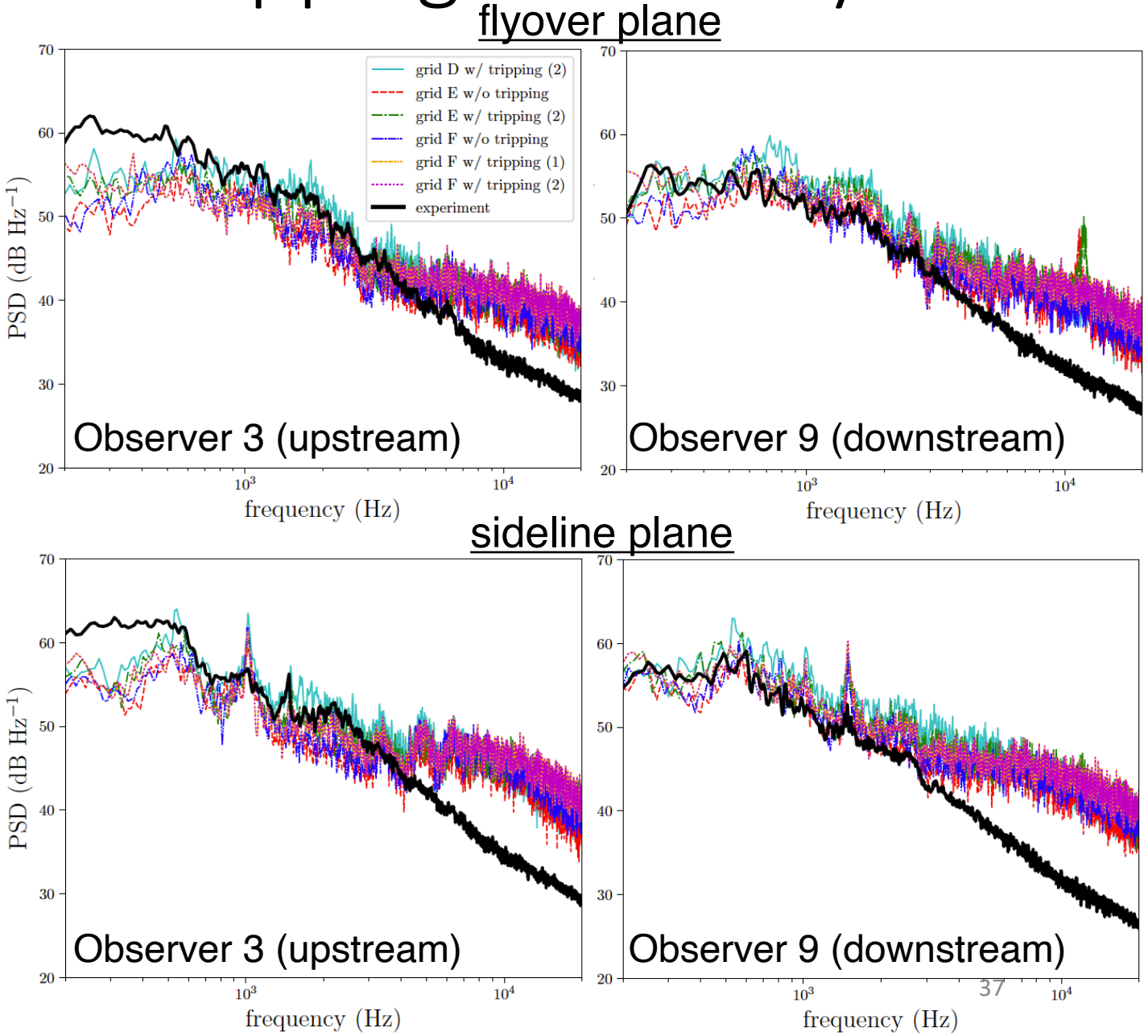
- Different cases **without** the tripping strips are compared
- For observer 9 that is located downstream of the landing gear, it can be seen from the plots that all numerical predictions compare reasonably well with the experimental results from 200 Hz to 4 kHz on both flyover and sideline planes
- Under-predictions similar to other works[1] seen in the noise levels below 500 Hz at upstream locations and these may be caused by unexpected wind tunnel noise, or noise diffraction at the nozzle lip since these observers are closer to the jet nozzle
- Over-predictions are observed in the higher frequency range in most of the simulations
- Surprisingly, low resolution grid B results agree well with the experimental measurements



1. Casalino, Damiano, et al. "Lattice–Boltzmann aeroacoustic analysis of the LAGOON landing-gear configuration." *AIAA journal* 52.6 (2014): 1232-1248.

Far-field Acoustics: Grid + Tripping Sensitivity

- The numerical tripping has insignificant effects on the low frequency noise
- In general, slightly more over-predictions in the high frequency range can be observed with tripping but the extra amount of over-predictions is small compared to those from the computations without tripping in the same frequency range.



Contradiction Observed & Outlook

- The far-field results obtained with low resolution CFD grid (grid B) are surprisingly good although poor predictions of the near-field pressure PSDs are seen, compared to the higher resolution cases

- On the other hand, the far-field results obtained with grids D, E and F have clear over-predictions in the high frequency range (> 4 kHz) while the near-field pressure PSD spectra are reasonably predicted

- Similar contradiction was also observed in the previous BANC-III workshop results with solid FWH approach, where the far-field predictions from simulations with different numerical and modeling approaches fit the experimental results well to more than 10 kHz using the solid FWH formulation, while the corresponding wall pressure PSD spectra are under-predicted below 2 kHz in general. This kind of contradiction is speculated to be caused by error cancellation in the integrals of the solid FWH formulation by Spalart et al.[1]

- The use of the permeable FWH method, which is a more general and correct approach for the far-field noise predictions will be examined

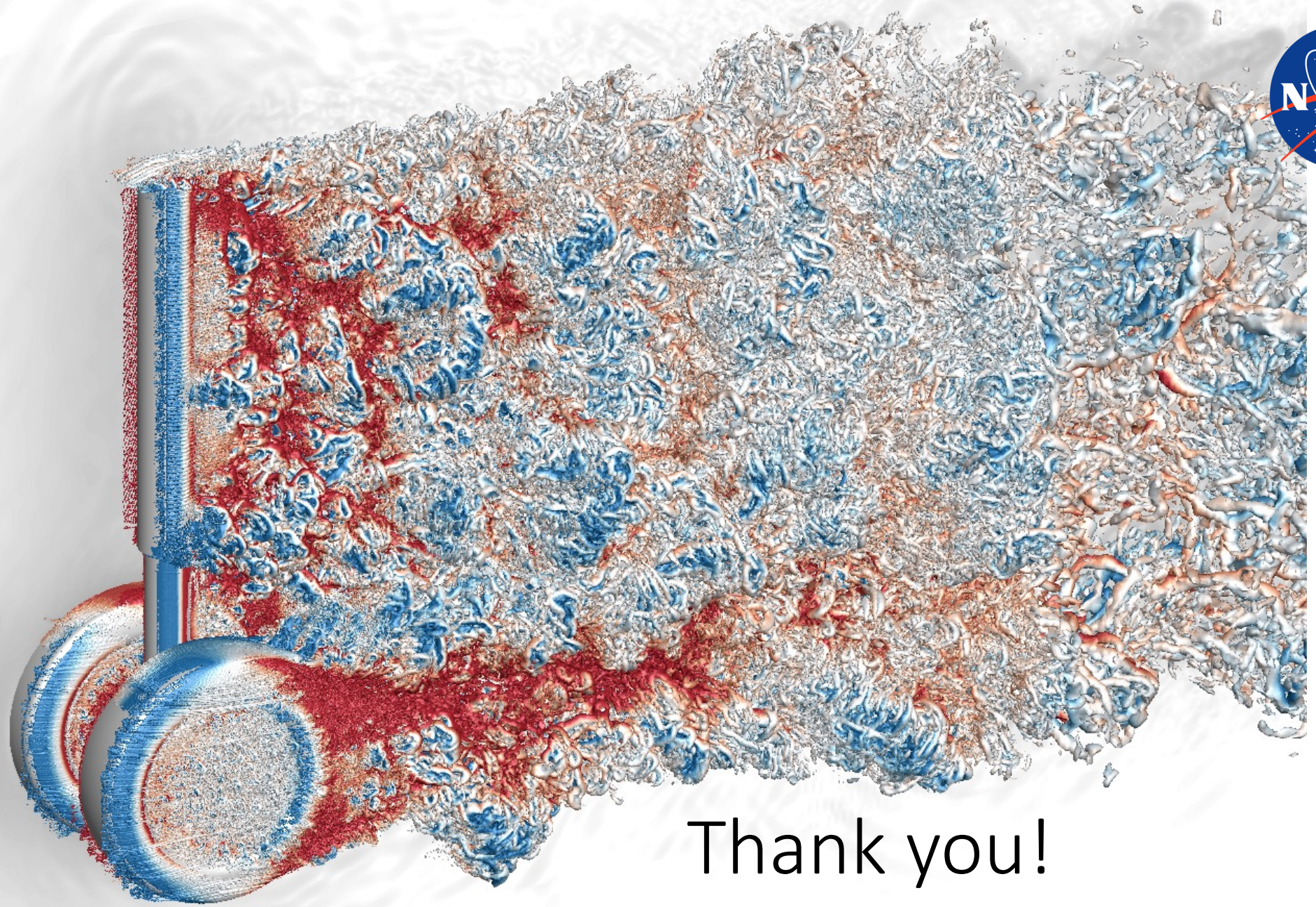
1. Spalart, P. R., Belyaev, K. V., Shur, M. L., Kh Strelets, M., and Travin, A. K., "On the differences in noise predictions based on solid and permeable surface Ffowcs Williams–Hawkings integral solutions," International Journal of Aeroacoustics, Vol. 18, No. 6-7, 2019, pp. 621–646.

Summary

- WMLES near-field and far-field results of the flow past a nose landing gear were studied and compared with experimental results
- The explicit modeling of the effects of tripping in experiments is necessary to reproduce laminar-to-turbulent transition in experiments for good comparison of near-field WMLES results with the experimental results
- With tripping:
  - Mean pressure coefficients at the axle and strut have smaller grid sensitivities
  - Pressure PSDs on the axle and strut components are also improved
  - The magnitudes and topologies of the mean velocity components in the turbulent wake were found to be closer to the experimental measurements
- However, the exact replication of tripping effects in the experiments is challenging due to the uncertainties of the small spatio-temporal scales involved
- Far-field results are not very sensitive to tripping by using the solid FWH acoustic analogy
- While there are reasonably good predications for far-field pressure PSDs up to 4 kHz, over-predictions in the spectrum levels were observed in the higher frequency range

Acknowledgments

- This work was partially funded by the NASA's Aeronautics Research Mission Directorate's (ARMD) Advanced Air Transport Technology (AATT) and Transformational Tools and Technologies (T^3)
- NASA Advanced Supercomputing (NAS) facility at NASA Ames Research Center
- Michael Barad, Jeffrey Housman, and other LAVA team members at NASA Ames Research Center for helpful discussions and advice
- Dr. Eric Manoha from ONERA for providing the geometry, experimental data, and documentations of the LAGOON benchmark problem



Thank you!

POC: manlong.wong@nasa.gov;
cetin.c.kiris@nasa.gov